peroxide (1:1). The solutions were evaporated to dryness on a hot plate and then, the residues were dissolved in dilute aqua regia (4 vol. %). Quantitative analysis of Pt for each solution was performed using inductively coupled plasma mass spectrometry (Model ELAN DRC II: Perkin Elmer SCIEX; Perkin Elmer Inc., Franklin, MA, USA).

Statistical analysis

Differences between the various treatments were statistically analysed using Student's *t*-test. For comparisons of multiple groups, one-way ANOVA was applied to the data. Furthermore, P values <0.05 were considered statistically significant. Data in the figures are shown as the mean ± SD of several experiments.

Results

Effects of nano-Pt on ROS production

We examined the effects of nano-Pt on UV-induced ROS production in keratinocytes. HaCaT cells were UV-treated with or without nano-Pt at different concentrations for 24 h, and flow cytometry with HE staining was used to detect ROS production in these cells. A marked increase in the production of O_2^- was observed 30 min after UV treatment in the cells. Nano-Pt at 100 μM concentration significantly inhibited each UV-induced O_2^- ($P \leq 0.001$) (Fig. S1). Therefore, we used nano-Pt at 100 μM concentration for next series of experiments. The percentage of cells producing O_2^- increased after UVA, UVB, and UVC irradiation dose dependently. Nano-Pt significantly inhibited UV-induced O_2^- [UVA 20 J/cm^2: 36.2 ± 2.1% ($P \leq 0.001$), UVB 60 mJ/cm^2: 26.0 ± 1.6% ($P < 0.05$), and UVC 60 mJ/cm^2: 42.7 ± 10.8% ($P \leq 0.001$)] (Fig. S1).

Effects of nano-Pt on UV-induced apoptosis

To investigate whether nano-Pt have the ability to protect against UV-induced apoptosis, HaCaT cells were UV-treated with or without nano-Pt (100 μM) for 24 h, and the effects were determined by evaluating DNA fragmentation in the cells. When these cells were pretreated with nano-Pt for 24 h, UVB- and UVC-induced apoptosis was significantly inhibited. On the other hand, nano-Pt had little effect on UVA-induced apoptosis, nano-Pt had only effective on 5 J/cm^2 UVA irradiation (Fig. 1). Annexin V-FITC-propidium iodide staining was used as a parameter for detecting apoptotic cell death, and the number of early apoptotic cells increased after UVB (20 and 40 mJ/cm^2) and UVC (20 and 40 mJ/cm^2) irradiation. Treatment with nano-Pt (100 μM) before UVB and UVC irradiation reduced the number of early apoptotic cells compared to UVB or UVC alone (Fig. 2). On the other hand, nano-Pt had no effect on UV-induced secondary necrosis.

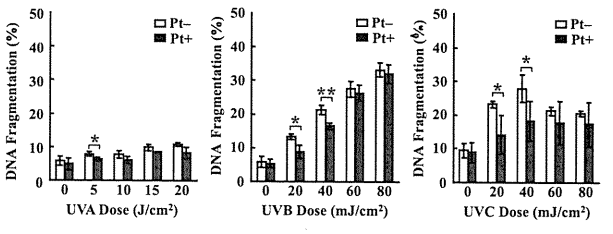

Figure 1. Effects of nano-Pt on ultraviolet-induced apoptosis. Cells were treated with UVA (5–20 J/cm^2), UVB (20–80 mJ/cm^2), and UVC (20–80 mJ/cm^2) with or without nano-Pt (100 μM) for 24 h. DNA fragmentation assay was performed after 24-h incubation at 37°C. Data are presented as mean ± SD (n = 5). *P < 0.05, **P ≤ 0.01. Data shown are representative of three independent experiments.

Expression of apoptosis-related proteins

Next, we evaluated changes in apoptotic marker proteins as a result of UV irradiation and exposure to nano-Pt (100 μM). The relative density of Bax, Bcl-X_L, and procaspase-3 to β-actin, calculated by integrating the density values of these three proteins, was similar in all the treated groups. The relative density of Bax to β-actin was 3.2 and 2.1 in samples irradiated with UVB and UVC, respectively. Nano-Pt decreased UVB- and UVC-induced Bax expression (UVB, 1.5; UVC, 1.7). The relative density of Bcl-X_L to β-actin was 0.08 in the UVB-irradiated samples. Furthermore, nano-Pt resulted in an increase in the UVB-induced Bcl-X_L expression (0.1) but did not alter the UVC-induced Bcl-X_L expression level. However, UVA irradiation did not alter Bax and Bcl-X_L expression levels. Expression of procaspase-3 decreased because of UVB and UVC irradiation and increased because of nano-Pt (Fig. 3). On the other hand, nano-Pt had no effect on Bax, Bcl-X_L, and procaspase-3 expression by UVA irradiation.

Effects of nano-Pt on Fas and the mitochondrial pathway

To examine the effects of nano-Pt on Fas externalization, cells were treated with or without 100 μM of nano-Pt for

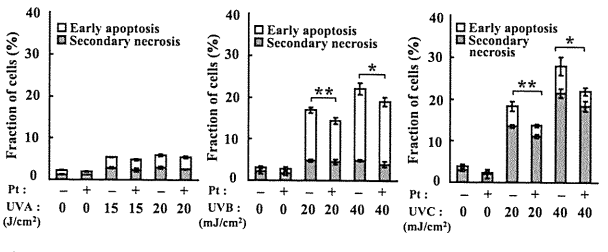

Figure 2. Effects of nano-Pt on ultraviolet (UV)-induced early apoptosis and secondary necrosis. Cells were treated with UVA, UVB, and UVC with or without nano-Pt (100 μM) for 24 h. Percentages of early apoptosis and secondary necrosis were analysed 24 h after UV treatment by flow cytometry. Data are presented as mean ± SD (n = 5). *$P \leq 0.05$, **$P \leq 0.01$. Data shown are representative of three independent experiments.

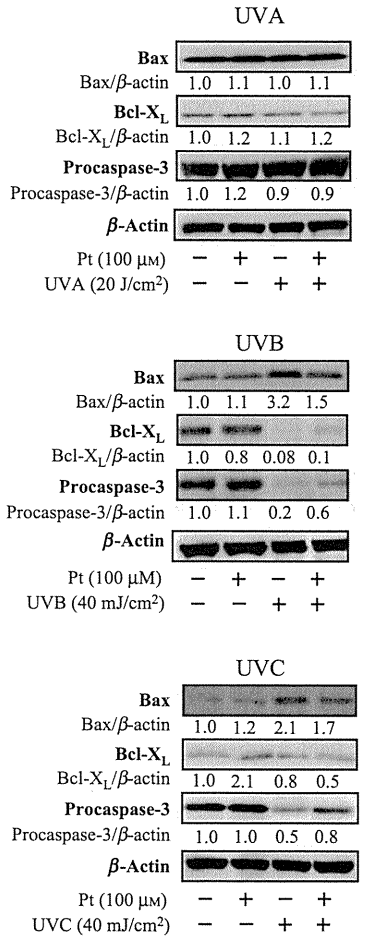

Figure 3. Ultraviolet-induced expression of apoptosis-related proteins. Immunoblot analysis of various apoptosis-related proteins in cells exposed to UVA, UVB, and UVC with or without nano-Pt (100 μM). Cell extracts were subjected to 5–20% SDS-PAGE and immunoblotted with antibodies against cleaved Bax, Bcl-X_L, caspase-3, and β-actin. Densitometry data, standardized by β-actin are presented below the band. Data shown are representative of three independent experiments.

24 h. Nano-Pt had no effect on UV-induced Fas production. Next, the effects of nano-Pt on the loss of mitochondrial membrane potential ($\Delta\Psi m$), which is an endpoint of apoptosis, were examined in HaCaT cells exposed to UV. Significant decrease in the loss of $\Delta\Psi m$ was observed (14.6 ± 3.1%; $P < 0.01$) when compared to UVB irradiation alone (Table 1).

Measurement of intracellular Pt content

When the intracellular content of Pt in samples was measured by inductively coupled plasma mass spectrometry, the values were 200 ng for treated cells and ≤0.05 ng for untreated control cells. Thus, intracellular incorporation of Pt was observed.

Table 1. Effects of nano-Pt endpoints of apoptosis

	Fas (%)	MMP (%)
Control	5.0 ± 0.1	5.0 ± 0.1
Pt + (100 μM)	5.1 ± 0.2	4.6 ± 0.4
UVA (20 J/cm^2)	21.6 ± 0.9	25.8 ± 1.6
Pt + UVA (20 J/cm^2)	20.7 ± 0.5	23.3 ± 2.0
UVB (40 mJ/cm^2)	15.6 ± 2.6	19.8 ± 1.2
Pt + UVB (40 mJ/cm^2)	13.2 ± 1.3	14.6 ± 3.1*
UVC (40 mJ/cm^2)	12.5 ± 2.8	9.6 ± 0.7
Pt + UVC (40 mJ/cm^2)	10.3 ± 1.7	9.2 ± 0.8

Cells were ultraviolet (UV) treated with or without nano-Pt (100 μM) for 24 h. The percentages of fraction of Fas positive cells are analyzed after UV treatment by flow cytometry using anti-Fas FITC antibody staining, and the percentages of loss of MMP are analyzed after UV treatment by flow cytometry using TMRM staining. The results are presented as the mean ± SD ($n = 5$).
*$P < 0.01$ vs UVB (40 mJ/cm^2).
MMP, mitochondrial membrane potential.

Effects of nano-Pt on UVB-mediated inflammation and apoptosis in mice

To present these results in an *in vivo* context, we analysed the role of nano-Pt ointment in UV-induced skin inflammation in mice. We assessed UVB irradiation–induced inflammation on the earlobes of mice. Twenty-four hours after 350 mJ/cm^2 UVB irradiation, the ear swelling in mice pretreated with nano-Pt gel was significantly decreased compared to that in UVB-irradiated control mice treated with carboxyvinyl gel polymer ($P < 0.01$) (Fig. S2). Immunochemical analysis demonstrated that a large number of TUNEL-positive cells were detected in the control mice after UVB irradiation, whereas few TUNEL-positive cells were detected in nano-Pt-treated mice ($P < 0.01$) (Fig. 5b,c). Thus, the nano-Pt-treated mice demonstrated a significantly smaller number of apoptotic cells than the control mice.

Effects of nano-Pt on photoallergy to LFLX plus UVA irradiation in mice

Subsequent studies were aimed to assess whether nano-Pt inhibit UVA-induced photoallergy. Fluoroquinolone photoallergy can be induced in Balb/c mice by sensitizing them by systemic administration of LFLX (2 mg/0.2 ml, i.p.), followed by 12 J/cm^2 UVA irradiation of the shaved abdomen, and posing a challenge using systemic quinolone and UVA exposure of the earlobes (20 J/cm^2). Significant ear swelling was observed in the positive control mice treated with carboxyvinyl polymer gel, but this response was inhibited in the earlobes of mice treated with nano-Pt gel prior to UVA irradiation ($P \leq 0.001$) (Fig. S3). Histological evaluation demonstrated that nano-Pt-treated mice had reduced cutaneous oedema, leucocyte infiltration, and hyperplasia even

on day 5 (Fig. S3). Northern blot analysis of the proinflammatory cytokine mRNA levels in the earlobes on day 5 showed decreased TNF-α, IL-1,β, and MIF expression in the nano-Pt-treated skin when compared to the positive control mouse skin (Fig. S3).

Discussion

UV irradiation of the skin results in a variety of injuries involving inflammatory and repair reactions, free radical reactions, and apoptosis. These injuries include immediate consequences, such as erythema and pigmentation, as well as delayed changes, such as cellular DNA mutations, hyperplasia, and carcinogenesis (17). ROS produced by UV radiation have the potential to damage critical cellular components, such as DNA, proteins, and lipids, eventually causing physical and chemical damage to skin tissues that may lead to cell death. To counteract oxidative injury, the skin is equipped with a network of enzymatic and non-enzymatic antioxidant systems, such as tocopherols and ascorbate polyphenols (18). This study demonstrated that treatment with nano-Pt reduced production of O_2^- in HaCaT cells before UV irradiation. Metal nanoparticles have been developed to increase the catalytic activity of metals because of the large surface area of smaller particles. Because nano-sized particles can reflect shorter wavelengths (UV light) (19), nanoparticles in the form of TiO_2 and ZnO have been used in sunscreen preparations to protect human skin physically. However, nano-Pt have been expected to protect human skin both physically and chemically owing to their SOD/catalase mimetic activity (8). Furthermore, compared to other metal nanoparticles, nano-Pt function as high reductive catalysts and may thus act as antioxidants to reduce ROS (8). Recently, Onizawa et al. demonstrated that treatment of alveolar-like A549 cells with nano-Pt inhibited cell death after exposure to a cigarette smoke extract. These results suggest that nano-Pt act as antioxidants that inhibit pulmonary inflammation induced by acute cigarette smoking (20). Furthermore, it has been demonstrated that nano-Pt prolonged the lifespan of worms, regardless of thermotolerance or dietary restriction (21). In this context, we suggest that nano-Pt are effective in reducing ROS production in UV-irradiated keratinocytes. Therefore, nano-Pt may have interesting anti-skin ageing properties.

Because DNA fragmentation, an endpoint of apoptosis, has been observed in human keratinocytes and HaCaT cells under certain conditions (22–24), we aimed at checking apoptosis-induction profile following different treatments using DNA fragmentation assay. The results revealed the occurrence of significant DNA fragmentation in HaCaT cells after UV irradiation. In this study, HaCaT cells irradiated with UVA, UVB, and UVC at different wavelengths demonstrated dose-dependent apoptosis following UVB and UVC exposure only, whereas no significant apoptosis was detected after UVA irradiation. Although UVA was shown to elevate intracellular superoxide production, it also induced delayed and sustained activation of extracellular signal-regulated kinase (ERK), which is apoptotic suppressor (25), and upregulation of the antiapoptotic protein Bcl-X_L by p38 MAPK activation (26). These simultaneous and opposing effects resulted in alleviation of the apoptotic stimulus. When HaCaT cells were irradiated with UVB and UVC in the presence of nano-Pt, UV-induced apoptosis was partially suppressed at 20 and 40 mJ/cm^2 in both cases. Because nano-Pt significantly attenuated superoxide formation in cells treated with UVA, UVB, and UVC but had no effect on peroxide formation, we concluded that superoxide plays an essential role in UVB- and UVC-induced apoptosis. It has been demonstrated that ROS increases the expression of cell surface Fas in human airway epithelial cells by promoting cytoplasmic transport of Fas (27). Thus, a putative mechanism of UVB- and UVC-induced apoptosis in HaCaT cells may involve accelerated recruitment of Fas on the cell membrane in response to elevated intracellular ROS, particularly superoxide, produced by UV irradiation. The apoptotic signal mediated by Fas guides the mitochondrial pathway and activation of caspase-3.

Similarly, our results demonstrated a significant increase in Fas expression and decrease in MMP in all UV-treated cells. On the other hand, a tendency for reduction in Fas expression and restoration of the decreased MMP content in the presence of nano-Pt was observed but was without statistical significance, except in case of UVB. When the Bcl-2 family proteins were measured, increased expression of the proapoptotic protein Bax and decreased expression of the antiapoptotic protein Bcl-X_L by UVB and UVC were reported. These effects were the opposite in the presence of nano-Pt. Furthermore, our data revealed caspase-3 activation by UV irradiation and its inhibition in the presence of nano-Pt. Therefore, the involvement of the mitochondrial caspase pathway and its modulation by intracellular superoxide in UV-induced apoptosis in HaCaT cells was confirmed. With respect to the localization of nanoparticles, Kiss et al. reported that TiO_2 nanoparticles cannot be uptaken by HaCaT cells (28). However, our results demonstrated the intracellular uptake of nano-Pt by HaCaT cells. Thus, we suggest that nano-Pt exerts protective effects because of their intracellular ROS scavenging activity.

The skin is continuously exposed to sunlight and environmental oxidizing pollutants; it is the preferred target of oxidative stress (29). Evidence suggests that signs of skin ageing, such as wrinkling, sagging, and actinic lentigines, may be associated with the cumulative oxidative damage incurred throughout our life. This study also demonstrates that nano-Pt gel applied topically on mouse skin protects against UVB-induced inflammation. Furthermore, we

demonstrated that nano-Pt have an antiapoptotic effect against UVB irradiation *in vivo*. UVB affects skin by inducing immunosuppression, premature skin ageing, inflammation, and cell death. Recent findings from our *in vivo* and *in vitro* observations suggest that nano-Pt can scavenge and inhibit inflammatory responses and apoptosis in the skin, which is caused by UVB exposure. Moreover, we found that nano-Pt gel was useful in mice with fluoroquinolone photoallergy. Fluoroquinolone photoallergy in mice is a model of photosensitivity dermatitis induced by UVA irradiation (30). Our results demonstrated that UVA-induced inflammation was clinically and histologically reduced by nano-Pt gel. Furthermore, proinflammatory cytokine levels in skin tissues decreased by nano-Pt treatment in mice with photoallergy. Sunscreens are recommended for protection against UV light–induced skin damage, but treatment of the skin with products containing antioxidant ingredients, such as tocopherols and ascorbate polyphenols, also be a useful strategy for the prevention of UV-mediated cutaneous damage. Broad-spectrum sunscreens are needed for protection against UVA. Therefore, it is suggested that nano-Pt demonstrating high antioxidant and antiinflammatory effects may have utility as a new class of sunscreens aimed at reducing ROS in the skin caused by UV exposure.

In conclusion, this study demonstrates that nano-Pt are effective in reducing UV-induced ROS and apoptosis and that topically applied nano-Pt effectively protects against UV-induced skin inflammation and photoallergy. Thus, we speculate that nano-Pt gel could be a useful sunscreen product for human skin therapy in the near future by providing effective protection against photo damage.

Acknowledgement

This research was supported by a Grant-in-Aid for research (No. 20591337) from the Ministry of Education, Science, and Culture of Japan.

Conflict of interest

The authors state no conflict of interest.

References

1 Peus D, Vasa R A, Meves A *et al.* H2O2 is an important mediator of UVB-induced EGF-receptor phosphorylation in cultured keratinocytes. J Invest Dermatol 1998: **110**: 966–971.
2 Ichihashi M, Ueda M, Budiyanto A *et al.* UV-induced skin damage. Toxicology 2003: **189**: 21–39.
3 Halliday G M. Inflammation, gene mutation and photoimmunosuppression in response to UVR-induced oxidative damage contributes to photocarcinogenesis. Mutat Res 2005: **571**: 107–120.
4 Bokov A, Chaudhuri A, Richardson A. The role of oxidative damage and stress in aging. Mech Ageing Dev 2004: **125**: 811–826.
5 Halliwell B. Antioxidant defence mechanisms: from the beginning to the end (of the beginning). Free Radic Res 1999: **31**: 261–272.
6 Saija A, Tomaino A, Trombetta D, Giacchi M, De Pasquale A, Bonina F. Influence of different penetration enhancers on in vitro skin permeation and in vivo photoprotective effect of flavonoids. Int J Pharm 1998: **175**: 85–94.
7 Casagrande R, Georgetti S R, Verri W A Jr, Dorta D J, dos Santos A C, Fonseca M J. Protective effect of topical formulations containing quercetin against UVB-induced oxidative stress. J Photochem Photobiol B 2006: **84**: 21–27.
8 Kajita M, Hikosaka K, Iitsuka M, Kanayama A, Toshima N, Miyamoto Y. Platinum nanoparticle is a useful scavenger of superoxide anion and hydrogen peroxide. Free Radic Res 2007: **41**: 615–626.
9 Boukamp P, Petrussevska R T, Breitkreutz D, Hornung J, Markham A, Fusenig N E. Normal keratinization in a spontaneously immortalized aneuploid human keratinocyte cell line. J Cell Biol 1998: **106**: 761–771.
10 Li F J, Kondo T, Zhao Q L *et al.* Enhancement of hyperthermia-induced apoptosis by a free radical initiator 2,2′-azobis (2-amidinopropane) dihydrochloride, in human histiocytic lymphoma U937 cells. Free Radic Res 2001: **35**: 281–299.
11 Sellins K S, Cohen J J. Gene induction by gamma-irradiation leads to DNA fragmentation in lymphocytes. J Immunol 1987: **139**: 3199–3206.
12 Hirano H, Tabuchi Y, Kondo T *et al.* Analysis of gene expression in apoptosis of human lymphoma U937 cells induced by heat shock and the effects of α-phenyl *N*-tert-butylnitrone (PBN) and its derivates. Apoptosis 2005: **10**: 331–340.
13 Zhao Q L, Fujiwara Y, Kondo T. Mechanism of cell death induction by nitroxide and hyperthermia. Free Radic Biol Med 2006: **40**: 1131–1143.
14 Lee E H, Faulhaber D, Hanson K M *et al.* Dietary lutein reduces ultraviolet radiation-induced inflammation and immunosuppression. J Invest Dermatol 2004: **122**: 510–517.
15 Tokura Y, Seo N, Yagi H, Furukawa F, Takigawa M. Cross-reactivity in murine fluoroquinolone photoallergy: exclusive usage of TCR Vbeta13 by immune T cells that recognize fluoroquinolone-photomodified cells. J Immunol 1998: **160**: 3719–3728.
16 Cui Z G, Kondo T, Ogawa R *et al.* Enhancement of radiation-induced apoptosis by 6-formylpterin. Free Radic Res 2004: **38**: 363–373.
17 Matsumura Y, Ananthaswamy H N. Toxic effects of ultraviolet radiation on the skin. Toxicol Appl Pharmacol 2004: **195**: 298–308.
18 Morganti P, Bruno C, Guarneri F, Cardillo A, Del Ciotto P, Valenzano F. Role of topical and nutritional supplement to modify the oxidative stress. Int J Cosmet Sci 2002: **24**: 331–339.
19 Sadrieh N, Wokovich A M, Gopee N V *et al.* Lack of significant dermal penetration of titanium dioxide (TiO_2) from sunscreen formulations containing nano- and sub-micron-size TiO_2 particles. Toxicol Sci 2010: **15**: 156–166.
20 Onizawa S, Aoshiba K, Kajita M, Miyamoto Y, Nagai A. Platinum nanoparticle antioxidants inhibit pulmonary inflammation in mice exposed to cigarette smoke. Pulm Pharmacol Ther 2009: **22**: 340–349.
21 Kim J, Takahashi M, Shimizu T *et al.* Effects of a potent antioxidant, platinum nanoparticle, on the lifespan of Caenorhabditis elegans. Mech Ageing Dev 2008: **129**: 322–331.
22 Woelfle U, Laszczyk M N, Kraus M *et al.* Triterpenes promote keratinocyte differentiation in vitro, ex vivo and in vivo: a role for the transient receptor potential canonical (subtype) 6. J Invest Dermatol 2009: **130**: 113–123.
23 Heinrich A, Balszuweit F, Thiermann H, Kehe K. Rapid simultaneous determination of apoptosis, necrosis, and viability in sulfur mustard exposed HaCaT cell cultures. Toxicol Lett 2009: **191**: 260–267.
24 Ayala F, Grimaldi E, Perfetto B *et al.* A 5-Aminolaevulinic acid and photodynamic therapy reduce HSV-1 replication in HaCat cells through an apoptosis-independent mechanism. Photodermatol Photoimmunol Photomed 2008: **24**: 237–243.
25 He Y -Y, Huang J -L, Colin CF. Delayed and sustained activation of extracellular signal-regulated kinase in human keratinocytes by UVA. J Biol Chem 2004: **279**: 53867–53874.
26 Bachelor M A, Bowden G T. Ultraviolet A-induced Modulation of Bcl-XL by p38 MAPK in Human Keratinocytes J Biol Chem 2004: **279**: 42658–42668.
27 Fujita A, Maruyama M, Araya J *et al.* Hydrogen peroxide induces upregulation of Fas in human airway epithelial cells via the activation of PARP-p53 pathway. Am J Respir Cell Mol Biol 2002: **27**: 542–552.
28 Kiss B, Bíró T, Czifra G *et al.* Investigation of micronized titanium dioxide penetration in human skin xenografts and its effect on cellular functions of human skin-derived cells. Exp Dermatol 2008: **17**: 659–667.
29 Thiele J J, Podda M, Packer L. Tropospheric ozone: an emerging environmental stress to skin. Biol Chem 1997: **378**: 1299–1305.
30 Tokura Y. Quinolone photoallergy: photosensitivity dermatitis induced by systemic administration of photohaptenic drugs. J Dermatol Sci 1998: **18**: 1–10.

Supporting Information

Additional Supporting Information may be found in the online version of this article:

Figure S1. Effects of nano-Pt on reactive oxygen species production.

Figure S2. Nano-Pt suppression of UVB-mediated inflammation in mice.

Figure S3. Nano-Pt suppression of photoallergy.

Please note: Wiley-Blackwell are not responsible for the content or functionality of any supporting materials supplied by the authors. Any queries (other than missing material) should be directed to the corresponding author for the article.

blood

2011 117: 3961-3967
Prepublished online February 16, 2011;
doi:10.1182/blood-2010-11-316794

Type of skin eruption is an independent prognostic indicator for adult T-cell leukemia/lymphoma

Yu Sawada, Ryosuke Hino, Kayo Hama, Shun Ohmori, Haruna Fueki, Shigenori Yamada, Shoko Fukamachi, Makiko Tajiri, Rieko Kubo, Manabu Yoshioka, Daiki Nakashima, Kazunari Sugita, Ryutaro Yoshiki, Takatoshi Shimauchi, Tomoko Mori, Kunio Izu, Miwa Kobayashi, Motonobu Nakamura and Yoshiki Tokura

Blood (print ISSN 0006-4971, online ISSN 1528-0020), is published weekly by the American Society of Hematology, 2021 L St, NW, Suite 900, Washington DC 20036.

Type of skin eruption is an independent prognostic indicator for adult T-cell leukemia/lymphoma

Yu Sawada,[1] Ryosuke Hino,[1] Kayo Hama,[1] Shun Ohmori,[1] Haruna Fueki,[1] Shigenori Yamada,[1] Shoko Fukamachi,[1] Makiko Tajiri,[1] Rieko Kubo,[1] Manabu Yoshioka,[1] Daiki Nakashima,[1] Kazunari Sugita,[1] Ryutaro Yoshiki,[1] Takatoshi Shimauchi,[1] Tomoko Mori,[1] Kunio Izu,[2] Miwa Kobayashi,[1] Motonobu Nakamura,[1] and Yoshiki Tokura[1,3]

[1]Department of Dermatology, University of Occupational and Environmental Health, Kitakyushu, Fukuoka, Japan; [2]Department of Dermatology, Kyushu Kosei Nenkin Hospital, Kitakyushu, Fukuoka, Japan; and [3]Department of Dermatology, Hamamatsu University School of Medicine, Hamamatsu, Shizuoka, Japan

Cutaneous involvement is seen in ~ 50% of adult T-cell leukemia/lymphoma (ATLL) patients. We investigated the association between skin eruption type and prognosis in 119 ATLL patients. ATLL eruptions were categorized into patch (6.7%), plaque (26.9%), multipapular (19.3%), nodulotumoral (38.7%), erythrodermic (4.2%), and purpuric (4.2%) types. When the T stage of the tumor-node-metastasis-blood (TNMB) classification of mycosis fungoides/Sézary syndrome was applied to ATLL staging, 16.0% were T1, 17.7% T2, 38.7% T3, and 4.2% T4, and the remaining 23.5% were of the multipapular and purpuric types. For the patch type, the mean survival time (median survival time could not be estimated) was 188.4 months. The median survival times (in months) for the remaining types were as follows: plaque, 114.9; multipapular, 17.3; nodulotumoral, 17.3; erythrodermic, 3.0; and purpuric, 4.4. Kaplan-Meier curves of overall survival showed that the erythrodermic type had the poorest prognosis, followed by the nodulotumoral and multipapular types. The patch and plaque types were associated with better survival rates. Multivariate analysis demonstrated that the hazard ratios of the erythrodermic and nodulotumoral types were significantly higher than that of the patch type, and that the eruption type is an independent prognostic factor for ATLL. The overall survival was worse as the T stage became more advanced: the multipapular type and T2 were comparable, and the purpuric type had a significantly poorer prognosis than T1. (*Blood*. 2011;117(15): 3961-3967)

Introduction

Adult T-cell leukemia/lymphoma (ATLL) is a malignancy of mature $CD4^+$ T cells caused by the human T-cell lymphotropic virus type I (HTLV-1).[1-3] HTLV-1 infection is prevalent in southern Japan, especially in Kyushu,[4,5] and in the Caribbean region and Africa.[6,7] Based on the number of abnormal lymphocytes, organ involvement, and severity, ATLL is divided into 4 clinical categories: acute, lymphoma, chronic, and smoldering (Shimoyama classification).[8] This classification is the most common tool used for estimating the prognosis of ATLL patients. The smoldering type has the best prognosis, followed by the chronic type, lymphoma type, and acute type. The median survival times (MSTs) of the acute, lymphoma, and chronic types are 6.2, 10.2, and 24.3 months, respectively.[8] Thus, the acute and lymphoma types of ATLL are associated with remarkably poor prognoses despite advances in chemotherapy and allogeneic hematopoietic stem cell transplantation.[9-11] In contrast, the chronic and smoldering types are relatively indolent and can usually be managed with "watchful waiting" until the disease progresses to acute crisis, just as smoldering (asymptomatic) myeloma is managed.[12]

Studies have attempted to identify other prognostic factors for survival of ATLL patients. Advanced performance status, high blood lactate dehydrogenase (LDH) level, age of 40 years or more, more than 3 involved lesions, and hypercalcemia have all been associated with shortened survival.[13] The existence of hepatosplenomegaly and lymphadenopathy also indicates poor prognosis.[8,14] However, there has been no large study on the correlation between the type and spread of skin eruptions and the prognosis of ATLL.

Because cutaneous involvement can be recognized in approximately 50% of ATLL patients,[15,16] the evaluation of skin lesions in relation to prognosis is important. Tumor cells infiltrating the skin exhibit several differences in phenotype and function.[17,18] ATLL patients can develop various types of eruptions, including nodules, tumors, plaques, erythrodermas, and even purpuric lesions,[19,20] and the categorization of these eruption types remains unclear. In this study, we retrospectively analyzed the prognosis of ATLL on the basis of the skin manifestations. We classified the skin eruptions and applied the T stage of the tumor-node-metastasis-blood (TNMB) classification for mycosis fungoides (MF) and Sézary syndrome (SS) to the type of skin lesions of ATLL. Our results indicate that eruption type is a predictor for prognosis.

Methods

Patients

We analyzed 119 patients with newly diagnosed, untreated ATLL who had skin eruptions and were seen at the University of Occupational and Environmental Health and Kyushu Kosei Nenkin Hospital from April 1979 to December 2009. The cutoff date for analysis was June 2010. The diagnosis of ATLL was based on clinical features, histopathologically and cytologically proven mature T-cell malignancy, presence of anti–HTLV-1 antibody, and monoclonal integration of HTLV-1 proviral DNA into the blood and/or skin tumor cells, as described previously.[2,8,21,22] The subtypes

Submitted November 5, 2010; accepted January 28, 2011. Prepublished online as *Blood* First Edition paper, February 16, 2011; DOI 10.1182/blood-2010-11-316794.

The publication costs of this article were defrayed in part by page charge payment. Therefore, and solely to indicate this fact, this article is hereby marked "advertisement" in accordance with 18 USC section 1734.

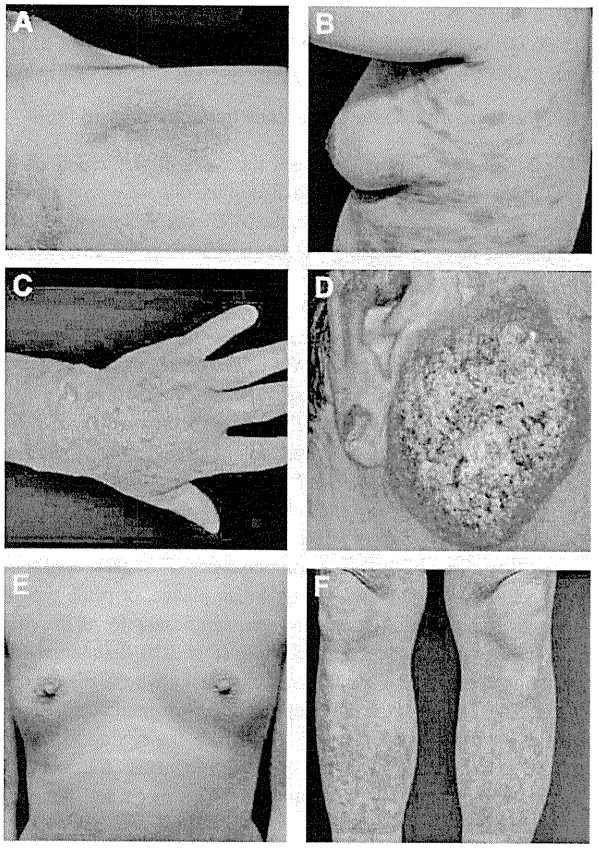

Figure 1. Clinical features of ATLL with skin eruptions. (A) Patch type, (B) plaque type, (C) multipapular type, (D) nodulotumoral type, (E) erythrodermic type, and (F) purpuric type.

of ATLL were classified according to the criteria established by the Lymphoma Study Group of Japan Clinical Oncology Group (Shimoyama classification).[8] Our retrospective, nonrandomized, observational study using existing data was granted an exemption from the institutional review board and was exempt from the requirement for written informed consent in accordance with the Declaration of Helsinki.

Clinical evaluation and definitions

The patients were categorized into 2 age groups: younger than 60 years and 60 years or older. Complications at diagnosis were classified into present and absent. Leukocytosis and lymphocytosis were defined as white blood cell count more than 12×10^9/L, and total lymphocyte count more than 6.5×10^9/L, respectively. LDH and calcium levels were classified into 2 groups according to a standard index.[13] We categorized skin eruptions of ATLL into 6 different types: patch, plaque, multipapular, nodulotumoral, erythrodermic, and purpuric (Figure 1). We defined the criteria for categorizing ATLL-related skin involvement into the patch type as no infiltrated erythema, the plaque type as infiltrated erythema, the multipapular type as multiple papules with diameter less than 1 cm, the nodulotumoral type as nodules or tumors with diameters more than 1 cm, the erythrodermic type as generalized erythema involving 80% or more of the patient's skin, and the purpuric type as red or purple discolorations that did not change with diascopy.

Statistical analyses

Overall survival (OS) was defined as the time from the date of first diagnosis to the date of death or the latest contact with the patient. Survival curves were drawn using the Kaplan-Meier method and were compared with the log-rank test. *P* values were calculated using the generalized Wilcoxon test. MST was defined as the time point at which the Kaplan-Meier survival curves crossed 50%. Mean survival time was provided when MST could not be calculated. To examine the multiple comparisons of the factors and of the pairs of groups, univariate and multivariate Cox regression analyses were applied to evaluate prognosis factors for survival. The effects of clinical parameters were evaluated as hazard ratios (HRs) and their 95% confidence intervals. All statistical analyses were performed using Dr SPSS II software (SPSS). A P value $< .05$ was considered statistically significant.

Results

Patient clinical characteristics

The clinical data of 119 patients with skin eruptions (ratio of male: female = 1.2:1) are summarized in Table 1. The mean age of the patients was 64.0 years (range, 23-91 years; SD, 12.00 years). According to Shimoyama classification, 40 (33.6%) patients were diagnosed with the acute type of ATLL, 6 (5.0%) with the chronic type, 17 (14.3%) with the lymphoma type, and 56 (47.1%) with the smoldering type. Twenty-three patients had complications at the time of diagnosis, including 7 patients with diabetes mellitus, 10 with hypertension, 3 with stroke, and 9 with opportunistic infections. Blood examination revealed that 36 patients (30.3%) had leukocytosis, 26 (21.9%) had lymphocytosis, and 49 (41.2%) had high LDH levels. Hypercalcemia was found in 70 patients (58.8%).

Patient skin lesions

We categorized the skin eruptions into the patch, plaque, multipapular, nodulotumoral, erythrodermic, and purpuric types (Figure 1). The most highly incident was the nodulotumoral type in 46 patients (38.7%), followed by the plaque type in 32 patients (26.9%), the multipapular type in 23 patients (19.3%), the patch type in 8 patients (6.7%), the erythrodermic type in 5 patients (4.2%), and the purpuric type in 5 patients (4.2%). Because the categorized skin eruptions of ATLL have similarities to those of MF/SS (with the exception of the multipapular and purpuric types), and because the TNMB classification for MF/SS[16] has been widely used, we attempted to apply the T stage of the TNMB classification to ATLL skin lesions. According to the MF/SS classification,[16] eruptions are classified into: T1 (patch/plaque, less than 10% of body surface), T2 (patch/plaque, more than 10% of body surface area), T3 (nodulotumoral type), and T4 (erythrodermic type). Ninety-one (76.5%) of our 119 patients could be classified using this system: 19 patients (16.0%) belonged to T1, 21 (17.7%) to T2, 46 (38.7%) to T3, and 5 (4.2%) to T4. The remaining 28 patients (23.5%) had multipapular (19.3%) and purpuric (4.2%) types, which are peculiar for ATLL and are not described in the T classification of MF/SS. We also evaluated these 2 types to investigate whether they are comparable with either the T1 or T4 category of the MF/SS classification system.

We examined the frequencies of the clinical subtypes of Shimoyama classification in each of the eruption types and T stages (Table 2). All patients with the erythrodermic type belonged to the acute type, whereas most of the patients with the patch type were grouped into the smoldering subtype. As the T stage advanced, the frequencies of the aggressive types (the acute and lymphoma types) increased, whereas those of the smoldering type decreased.

Survival by baseline clinical factors

Sixty-nine of our 119 patients died during the observation period, with a median follow-up duration of 3.0 years (range, 30 days-20.3 years). The MSTs of the acute, lymphoma, chronic, and

Table 1. Survival by baseline clinical factors

Factor	No. of evaluated cases	No. of deaths	MST, mos	P
Total	119	69		
Clinical subtype				< .001
Acute type	40	30	7.7	
Lymphoma type	17	12	15.0	
Chronic type	6	5	16.6	
Smoldering type	56	22	154.0	
Patient-related factors				
Sex				.956
Male	66	38	20.3	
Female	53	31	24.9	
Age, y				.702
≥ 60	81	46	24.5	
< 60	38	23	18.4	
Complications at diagnosis				.114
Absent	96	59	21.0	
Present				
Diabetes mellitus	7	3	14.8	
Hypertension	10	4	141.4*	
Stroke	3	2	17.2	
Opportunistic infections	9	4	49.3	
Hematologic factors				
WBC count, × 10^9/L				< .001
≥ 12.0	36	25	9.5	
< 12.0	83	44	47.8	
Total lymphocyte count, × 10^9/L				< .001
≥ 6.5	26	20	10.4	
< 6.5	93	49	47.8	
Laboratory factors				
LDH				< .001
≤ NI	70	37	47.9	
> NI	49	32	9.5	
Calcium				.420
≤ NI	49	28	27.8	
> NI	70	41	18.6	
Skin lesions				< .001
Patch type	8	2	188.4*	
Plaque type	32	9	114.9	
Multipapular type	23	12	17.3	
Nodulotumoral type	46	38	17.3	
Erythrodermic type	5	5	3.0	
Purpuric type	5	3	4.4	
T stage				< .001
T1	19	3	192.6*	
T2	21	8	47.9	
T3	46	38	17.3	
T4	5	5	3.0	

The cumulative probability of the survival rate was estimated using the Kaplan-Meier method and the *P* value was calculated using the generalized Wilcoxon test.

MST indicates median survival time; and NI, normal index.

*Mean survival time is given because the MST cannot be calculated.

smoldering types were 7.7, 15.0, 16.6, and 154.0 months, respectively (Table 1). Of the 69 fatal cases during the observation, 45 patients died of acute ATLL, 17 of acute crisis from the other subtypes, 5 of other diseases (3 of chronic pulmonary diseases and 2 of acute respiratory disease syndrome [ARDS]), and 2 patients of unknown causes.

The effects of various clinical factors on prognosis in the 119 patients were analyzed using the Kaplan-Meier method (Table 1). There was no statistically significant difference in survival rates between the absence and presence of any complication ($P = .114$), between the ≥ 60 years and < 60 years age groups ($P = .702$), or between males and females ($P = .956$). The survival rate was poor in patients with leukocytosis ($P < .001$), lymphocytosis ($P < .001$), and higher LDH levels ($P < .001$). Blood calcium level did not significantly affect survival in this study.

Survival and multivariate analyses in each eruption type

The MSTs were different between the types of skin eruptions. In the erythrodermic type, all 5 patients died of the disease with 3.0 months of MST. In the nodulotumoral type, the MST was 17.3 months, and 38 of 46 patients died, 17 of acute ATLL, 16 of acute crisis, 1 of ARDS, 2 of chronic pulmonary disease, and 2 of unknown causes. In the plaque type, the MST was 114.9 months, and 9 of 32 died of the disease. The multipapular type showed the same MST (17.3 months) as the nodulotumoral type, and 9 died of acute ATLL, 1 of acute crisis, 1 of ARDS, and 1 of chronic pulmonary disease. The patch type exhibited a good prognosis, with 188.4 months of mean survival time (the MST was not estimable). The purpuric type was found to have a poor prognosis, with an MST of 4.4 months and 3 of 5 patients dying of the disease.

Kaplan-Meier curves of the OS for each eruption type are shown in Figure 2A. The OS rate of the erythrodermic type was significantly lower than those of the other eruption types ($P < .001$, erythrodermic type vs the nodulotumoral, multipapular, plaque, or patch types). The OS rate of the nodulotumoral type was significantly lower than those of the multipapular, plaque, or patch types ($P = .010$, nodulotumoral type vs multipapular type; $P < .001$, nodulotumoral type vs plaque or patch type). The OS rate of the multipapular type was significantly lower than that of the patch type ($P = .045$). Therefore, the erythrodermic type of ATLL is associated with the poorest prognosis, followed by the nodulotumoral and multipapular types. The patch and plaque types showed better survival rates.

We performed univariate and multivariate analyses of the eruption types in a comparison with Shimoyama classification, sex, age, complications, leukocyte counts, lymphocyte counts, LDH level, and calcium level (Table 3). In the multivariate analysis, the smoldering type proved to be a good prognostic factor. We fixed the HR of the patch type to be 1, and then compared it with those of the other eruption types. In the univariate analysis, the HRs of the other eruption types were significantly higher than that of the patch type. In the multivariate analysis, the HRs of the nodulotumoral and erythrodermic types were significantly higher than that of the patch type. The purpuric type also showed such a tendency; however, this result provided limited power for tests against the other groups. The analysis demonstrated that the eruption type is an independent prognostic factor for ATLL.

Survival and univariate and multivariate analyses in each T stage

We also performed the univariate and multivariate analyses of T stage and other clinical and laboratory parameters for OS. Of 19 patients in the T1 stage, 3 died of the disease, and the mean survival time (the MST was not estimable) was 192.6 months (Table 1). In the T2 stage, 8 of 21 died of the disease and the MST was 47.9 months. In the T3 stage, the MST was 17.3 months and 38 of 46 patients died: 17 of acute ATLL, 16 of acute crisis, 1 of ARDS, 2 of chronic pulmonary disease, and 2 of unknown etiology. In the T4 stage, 5 patients died of the disease with 3.0 months of MST. The OS of the patients was worse as the T stage became more advanced (Figure 2B). Patients in the T1 stage had the longest OS, followed by patients in the T2-T4 stages ($P = .034$, T1 vs T2; $P < .001$, T1 vs T3 or T4; $P < .001$ T2 vs T3 or T4; and $P < .001$, T3 vs T4).

The multipapular and purpuric types are missing in the T stage of the MF/SS system due to their peculiarity. We therefore compared the OS of

Table 2. Frequencies of the clinical types of Shimoyama classification in each eruption type and T stage

	Acute type	Lymphoma type	Chronic type	Smoldering type	*P*
Eruption type					.015
Patch type	0	0	1 (12.8%)	7 (87.2%)	
Plaque type	9 (28.1%)	4 (12.5%)	0	19 (59.4%)	
Multipapular type	10 (43.5%)	2 (8.7%)	0	11 (47.8%)	
Nodulotumoral type	14 (30.4%)	10 (21.7%)	5 (10.9%)	17 (37.0%)	
Erythrodermic type	5 (100%)	0	0	0	
Purpuric type	2 (40.0%)	1 (20.0%)	0	2 (40.0%)	
T stage					.004
T1	2 (10.5%)	1 (5.3%)	0	16 (84.2%)	
T2	7 (33.3%)	3 (14.3%)	1 (4.8%)	10 (47.6%)	
T3	14 (30.4%)	10 (21.7%)	5 (10.9%)	17 (37.0%)	
T4	5 (100%)	0	0	0	

these 2 eruption types with those of the T stages. Patients with the multipapular type and T2 had a similar outcome (Figure 2C), and there was no statistical significance ($P = .415$). Patients with the purpuric type had a significantly poorer prognosis than those with T1 ($P = .001$); Figure 2D). The differences in OS between the purpuric type and the other T stages were not statistically significant ($P = .412$, purpuric type vs T2; $P = .257$; purpuric type vs T3; $P = .099$, purpuric type vs T4).

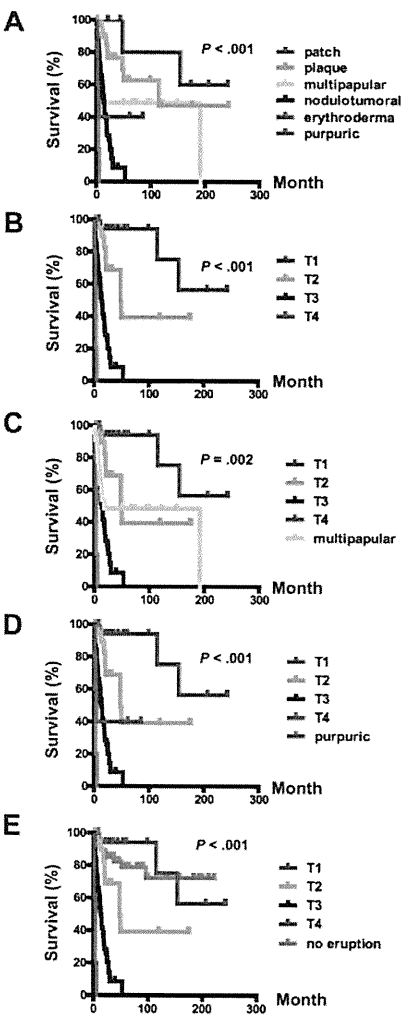

Figure 2. OS of ATLL patients with skin eruptions. (A) OS rates of skin eruption types. (B) OS rate of T stage. (C) OS rate of the T stage and the multipapular type. (D) OS rate of the T stage and the purpuric type. (E) OS rate of the T stage and the no-eruption type.

We performed univariate and multivariate analyses of T stage and clinical and laboratory parameters with the HR of T1 set as 1 (Table 3). The univariate analysis revealed that the prognoses of T2, T3, T4, and the multipapular and purpuric types were significantly higher than that of T1. In the multivariate analysis, the HR of T3 and T4 and the multipapular and purpuric types were significantly higher than that of T1.

Survival and univariate and multivariate analyses in each T stage and in the no-eruption group

We performed univariate and multivariate analyses of T stage by comparing them with the no-eruption group and other clinical and laboratory parameters for OS. Of 51 patients without skin eruptions, 10 died of the disease and the mean survival time (the MST was not estimable) was 66.5 months. When classifying the no-eruption patients into each clinical Shimoyama subtype, 7 patients (13.7%) belonged to the acute type, 5 (9.8%) to the lymphoma type, 12 (23.5%) to the chronic type, and 27 (52.9%) to the smoldering type. The OS of the patients without eruption was better than those at T2-T4 (Figure 2E; no-eruption group vs T2, $P = .033$; no eruption group vs T3 or T4, $P < .001$). There was no statistically significant difference in OS between the no-eruption group and T1.

We performed univariate and multivariate analyses of T stage, including the no-eruption group and clinical and laboratory parameters, by assigning a value of 1 to the HR of T1 (Tables 4 and 5). The univariate and multivariate analyses revealed that the prognoses of T3 and T4 were significantly worse than that of T1.

Discussion

In the present study, we investigated the association of each type of skin eruption with prognosis in ATLL patients and attempted to apply the T stage of MF/SS classification to the assessment of ATLL skin lesions. We classified ATLL skin eruptions into 6 categories: patch, plaque, multipapular, nodulotumoral, erythrodermic, and purpuric. Table 2 shows that the frequencies of the clinical subtypes of Shimoyama classification were different for each eruption type and T stage. All erythrodermic patients belonged to the acute type, whereas most of patients with the patch type were of the smoldering type. This raised the possibility that prognosis is different among the individual eruption types. Our results revealed the poorest prognosis in the erythrodermic type, followed by the nodulotumoral and multipapular types. The patch and plaque types exhibited better survival rates. Moreover, our multivariate analysis demonstrated that the HRs of the erythrodermic and nodulotumoral

Table 3. Cox analysis of eruption type and T stage for clinical factors and OS

	Univariate		Multivariate (eruption type and clinical factors)		Multivariate (T stage and clinical factors)	
Clinical factor	**HR (95% CI)**	***P***	**HR (95% CI)**	***P***	**HR (95% CI)**	***P***
Clinical subtype						
Acute type	1		1		1	
Lymphoma type	0.5 (0.1-0.8)	.013	0.9 (0.3-2.5)	.852	0.9 (0.1-1.3))	.852
Chronic type	0.1 (0.3-1.1)	.082	0.4 (0.1-1.4)	.167	0.4 (0.3-2.4)	.140
Smoldering type	0.1 (0.1-0.2)	< .001	0.2 (0.8-0.6)	.002	0.2 (0.1-0.6)	.003
Patient-related factors						
Sex						
Male	1		1		1	
Female	1.0 (0.6-1.6)	.903	1.2 (0.7-2.1)	.576	1.2 (0.7-2.1)	.576
Age, y						
< 60	1		1		1	
≥ 60	1.0 (0.6-1.7)	.922	0.9 (0.5-1.6)	.658	0.9 (0.5-1.5)	.578
Complications at diagnosis						
Absent	1		1		1	
Present						
Diabetes mellitus	0.6 (0.2-2.0)	.427	0.5 (0.1-1.9)	.314	0.5 (0.1-1.8)	.274
Hypertension	0.4 (0.2-1.2)	.119	1.0 (0.3-3.9)	.958	1.1 (0.3-4.2)	.905
Stroke	1.8 (0.4-7.3)	.425	3.5 (0.6-19.4)	.161	2.9 (0.5-17.3)	.256
Opportunistic infection	1.0 (0.4-2.6)	.927	1.0 (0.3-3.1)	.958	1.1 (0.3-3.4)	.938
Hematologic factors						
WBC count, × 10^9/L						
< 12.0	1		1		1	
≥ 12.0	3.6 (2.1-6.2)	< .001	1.8 (0.6-5.2)	.279	1.7 (0.6-4.9)	.325
Total lymphocyte count, × 10^9/L						
< 6.5	1		1		1	
≥ 6.5	3.7 (2.0-6.5)	< .001	1.1 (0.5-2.6)	.803	1.1 (0.5-2.7)	.768
Laboratory factors						
LDH						
≤ NI	1		1		1	
> NI	3.0 (1.8-4.9)	< .001	1.2 (0.6-2.2)	.581	1.2 (0.6-2.2)	.599
Calcium						
≤ NI	1		1		1	
> NI	1.3 (0.8-2.1)	.381	1.0 (0.6-1.8)	.960	1.0 (0.6-1.8)	.914
Eruption type						
Patch	1		1			
Plaque	2.2 (0.5-10.9)	.321	1.4 (0.3-8.0)	.680		
Nodulotumoral	12.5 (2.7-57.1)	.001	8.8 (1.6-48.0)	.012		
Erythrodermic	68.4 (11.5-405.9)	< .001	21.2 (3.0-150.3)	.002		
Multipapular	4.8 (1.0-22.6)	.045	3.5 (0.6-20.1)	.159		
Purpuric	7.1 (1.1-45.7)	.039	6.8 (0.9-53.7)	.071		
T stage						
T1	1				1	
T2	4.0 (1.0-15.1)	.047			2.2 (0.5-9.8)	.304
T3	15.3 (4.4-52.8)	< .001			11.3 (2.8-46.0)	.001
T4	83.9 (17.8-394.6)	< .001			27.5 (5.0-151.8)	< .001
Multipapular type	5.8 (1.6-20.9)	.007			8.1 (1.4-47.1)	.045
Purpuric type	8.6 (1.7-44.5)	.010			8.1 (1.4-47.1)	.020

CI indicates confidence interval; and NI, normal index.

types were significantly higher than that of the patch type, and that skin eruption is an independent prognostic factor for ATLL.

Table 4. Univariate analyses of T stage compared with patients having no skin eruptions

	Univariate	
Clinical factor	**HR (95% CI)**	***P***
T stage		
T1	1	
T2	3.6 (0.9-13.6)	.059
T3	16.4 (4.9-55.1)	< .001
T4	127.4 (26.2-618.1)	< .001
No eruption	1.3 (0.3-4.8)	.670

It has been reported that the smoldering type of ATLL with skin eruptions, especially those of the nodulotumoral type, has a poorer prognosis than ATTL without skin involvement.[19] Another group of investigators reported that the MSTs of the nodulotumoral and maculopapular types were 26 and 80 months, respectively, which are significantly shorter than those in ATLL without cutaneous eruptions.[23] Our findings are in agreement with these observations, and further clarify the relationship between type of skin lesion and prognosis. Skin-targeted therapy using topical steroids, psoralen photochemotherapy, or narrow-band UVB therapy[19] may improve the prognosis of ATLL for patients with skin eruptions.

The purpuric type of ATLL is one of the rarest skin eruptions of ATLL,[24] and has been reported to occur in 1.6% of ATLL patients with

Table 5. Cox multivariate analyses of clinical factors and OS compared with patients having no eruption

	Multivariate	
Clinical factor	**HR (95% CI)**	***P***
Clinical subtype		
Acute type	1	
Lymphoma type	2.4 (0.8-7.2)	.110
Chronic type	0.3 (0.1-0.9)	.036
Smoldering type	0.4 (0.1-1.1)	.068
Patient-related factors		
Sex		
Male	1	
Female	0.8 (0.4-1.4)	.440
Age, y		
< 60	1	
≥ 60	0.4 (0.2-0.8)	.012
Complications at diagnosis		
Absence	1	
Presence		
Diabetes mellitus	1.9 (0.7-4.8)	.188
Hypertension	0.6 (0.2-2.1)	.443
Stroke	2.6 (0.6-10.5)	.191
Opportunistic infection	1.1 (0.2-6.1)	.925
Hematologic factors		
WBC count, × 10^9/L		
< 12.0	1	
≥ 12.0	1.1 (0.3-3.5)	.864
Total lymphocyte count, × 10^9/L		
< 6.5	1	
≥ 6.5	2.0 (0.7-5.9)	.197
Laboratory factors		
LDH		
≤ NI	1	
> NI	1.2 (0.7-2.1)	.596
Calcium		
≤ NI	1	
> NI	1.1 (0.6-1.9)	.826
T stage		
T1	1	
T2	2.4 (0.6-9.7)	.227
T3	13.4 (3.3-53.9)	< .001
T4	60.8 (10.1-366.4)	< .001
No eruption	0.9 (0.2-3.6)	.847

CI indicates confidence interval; and NI, normal index.

skin lesions.[19] However, its incidence is higher than was previously thought, because we documented a 4.2% frequency in this study. The production of granzyme B by ATLL cells may lead to the destruction of vessels and the development of purpuric eruptions in these patients.[24] The prognosis for the purpuric type of skin lesion has not been investigated because of the rarity of this type. There have been 9 cases of the purpuric type reported in the literature.[24-31] When these are divided into the punctate and macular subtypes, the prognosis of the punctate purpuric subtype might be better than the macular purpuric subtype.[24-31] In our 5 purpuric cases, 2 cases of the punctuate purpuric subtype survived, with a 73.4-month mean survival time (the MST was not estimable), whereas 3 cases of the macular purpuric subtype died with 2.1 months of the MST. This suggests that the punctuate subtype has a good clinical prognosis, and the poor prognosis of the total purpuric type is derived from the macular subtype.

In addition to the purpuric type, the erythrodermic type is a rare skin manifestation in ATLL patients, with a prevalence of 3.5% reported in a previous study[19] and 4.2% in the present study. The majority of ATLL cases associated with the erythrodermic type of skin lesion are aggressive. In our study, all patients with erythrodermic lesions also belonged to the acute type and had the poorest prognosis among all skin eruption types. In patients with cutaneous T-cell lymphoma (CTCL), the erythrodermic type is typically termed SS and also has a poor prognosis.[16] In some erythrodermic CTCL patients, the decreased expression of intercellular adhesion molecule-1 by keratinocytes may lead to an inability of malignant T cells to enter the epidermis and infiltrate the blood and other organs.[32] This pathomechanism in erythrodermic CTCL can also be applied to ATLL, resulting in poor prognosis. Skin biopsy specimens of the erythrodermic type of ATLL revealed scant tumor cell infiltration into the epidermis.[33,34]

We applied MF/SS classification T stages to ATLL assessment, and demonstrated that the OS was worse as the T stage became more advanced. The results shown in Table 3 indicated that the prognosis of T1 stage was better than that for T2, suggesting that the difference in the body surface area of skin lesions is associated with the prognosis of ATLL. Moreover, the prognosis of T3 patients was poorer than those of T1 and T2, indicating that the depth of tumor-cell infiltration is associated with survival rate. T-stage classification accurately reflects the prognosis of ATLL and MF/SS. However, the multipapular and purpuric types are not applicable to T stage. We found that the multipapular type and T2 had similar outcomes, and that the purpuric type had a significantly poorer prognosis than T1. This may provide clinically useful information for patient management and choice of therapy. Moreover, our present study demonstrated that skin eruption is an independent prognostic factor for ATLL patients: the presence of skin eruptions may indicate poorer outcome compared with no eruptions. Therefore, evaluation of skin lesions and treatments targeting the skin may be important for improving clinical outcome.

Acknowledgments

We thank R. Ide (Department of Work Systems and Health, Institute of Industrial Ecological Sciences, University of Occupational and Environmental Health) and Y. Miyamura (Department of Environmental Epidemiology, University of Occupational and Environmental Health) for advising on the statistical analyses.

This work was supported by Grants-in-Aid for Science Research from the Ministry of Education, Science, Sports, and Culture of Japan.

Authorship

Contribution: Y.S. collected and analyzed the data and wrote the manuscript; R.H. analyzed the data; K.H. collected the data; S.O., H.F., S.Y., S.F., M.T., R.K., M.Y., D.N., K.S., R.Y., T.S., T.M., K.I., M.K., and M.N. diagnosed and treated ATLL patients; and Y.T. organized the study.

Conflict-of-interest disclosure: The authors declare no competing financial interests.

Correspondence: Yu Sawada, MD, Department of Dermatology, University of Occupational and Environmental Health, 1-1 Iseigaoka, Yahatanishi-ku, Kitakyushu 807-8555, Japan; e-mail: longago@med.uoeh-u.ac.jp; or Ryosuke Hino, MD, PhD, Department of Dermatology, University of Occupational and Environmental Health, 1-1 Iseigaoka, Yahatanishi-ku, Kitakyushu 807-8555, Japan; e-mail: hinoti@med.uoeh-u.ac.jp.

References

1. Uchiyama T, Yodoi J, Sagawa K, et al. Adult T-cell leukemia: clinical and hematologic features of 16 cases. *Blood.* 1977;50(3):481-492.
2. Yoshida M, Miyoshi I, Hinuma Y. Isolation and characterization of retrovirus from cell lines of human adult T-cell leukemia and its implication in the disease. *Proc Natl Acad Sci U S A.* 1982; 79(6):2031-2035.
3. Tsukasaki K, Hermine O, Bazarbachi A, et al. Definition, prognostic factors, treatment, and response criteria of adult T-cell leukemia-lymphoma: a proposal from an international consensus meeting. *J Clin Oncol.* 2009;27(3):453-459.
4. Iwanaga M, Chiyoda S, Kusaba E, Kamihira S. Trends in the seroprevalence of HTLV-1 in Japanese blood donors in Nagasaki Prefecture, 2000-2006. *Int J Hematol.* 2009;90(2):186-190.
5. Tajima K. The 4th nation-wide study of adult T-cell leukemia/lymphoma (ATL) in Japan: estimates of risk of ATL and its geographical and clinical features. The T- and B-cell Malignancy Study Group. *Int J Cancer.* 1990;45(2):237-243.
6. Levine PH, Blattner WA, Clark J, et al. Geographic distribution of HTLV-I and identification of a new high-risk population. *Int J Cancer.* 1988; 42(1):7-12.
7. Fleming AF, Maharajan R, Abraham M, at al. Antibodies to HTLV-I in Nigerian blood-donors, their relatives and patients with leukaemias, lymphomas and other diseases. *Int J Cancer.* 1986; 38(6):809-813.
8. Shimoyama M. Diagnosis criteria and classification of clinical subtypes of adult T-cell leukemia-lymphoma: a report from the Lymphoma Study Group. *Br J Hematol.* 1991;79(3):428-437.
9. Yamada Y, Tomonaga M, Fukuda H, et al. A new G-CSF-supported combination chemotherapy, LGS15, for adult T-cell leukemia-lymphoma: Japan Clinical Oncology Group Study 9303. *Br J Haematol.* 2001;113(2):375-382.
10. Fukushima T, Miyazaki Y, Honda S, et al. Allogenic hematopoietic stem cell transplantation provides sustained long-term survival for patients with adult T-cell leukemia/lymphoma. *Leukemia.* 2005;19(5):829-834.
11. Tsukasaki K, Utsunomiya A, Fukuda H, et al. VCAP-AMP-VECP compared with biweekly CHOP for adult T-cell leukemia-lymphoma: Japan clinical oncology group study JCOG 9801. *J Clin Oncol.* 2007;25:5458-5464.
12. Bladé J, Dimopoulos M, Rosiñol L, Rajkumar SV, Kyle RA. Smoldering (asymptomatic) multiple myeloma: current diagnostic criteria, new predictors of outcome, and follow-up recommendations. *J Clin Oncol.* 2010;28(4):690-697.
13. Lymphoma Study Group. Major prognostic factors of patients with adult T-cell leukemia-lymphoma: a cooperative study. Lymphoma Study Group (1984-1987). *Leuk Res.* 1991;15(2-3):81-90.
14. Broder S. NIH conference: T-cell lymphoproliferative syndrome associated with human T-cell leukemia/lymphoma virus. *Ann Intern Med.* 1984; 100(4):543-557.
15. Yamaguchi T, Ohshima K, Karube K, et al. Clinicopathological features of cutaneous lesions of adult T-cell leukaemia/lymphoma. *Br J Dermatol.* 2005;152(1):76-81.
16. Willemze R, Jaffe ES, Burg G, et al. WHO-EORTC classification for cutaneous lymphomas. *Blood.* 2005;105(10):3768-3785.
17. Shimauchi T, Imai S, Hino R, Tokura Y. Production of thymus and activation-regulated chemokine and macrophage-derived chemokine by CCR4+ adult T-cell leukemia cells. *Clin Cancer Res.* 2005;11(6):2427-2435.
18. Shimauchi T, Kabashima K, Nakashima D, et al. Augmented expression of programmed death-1 in both neoplastic and non-neoplastic CD4+ T-cells in adult T-cell leukemia/lymphoma. *Int J Cancer.* 2007;121(12):2585-2590.
19. Setoyama M, Katahira Y, Kanzaki T. Clinicopathologic analysis of 124 cases of adult T-cell leukemia/lymphoma with cutaneous manifestations: the smouldering type with skin manifestations has a poorer prognosis than previously thought. *J Dermatol.* 1999;26(12):785-790.
20. Chan HL, Su IJ, Kuo T, et al. Cutaneous manifestations of adult T-cell leukemia/lymphoma. Report of three different forms. *J Am Acad Dermatol.* 1985;13(2, pt 1):213-219.
21. Yamada Y. Phenotypic and function analysis of leukemic cells from 16 patients with adult T-cell leukemia/lymphoma. *Blood.* 1983;61(1):192-199.
22. Tsukasaki K, Ikeda S, Murata K, et al. Characteristics of chemotherapy-induced clinical remission in long survivors with aggressive adult T-cell leukemia/lymphoma. *Leuk Res.* 1993;17(2):157-166.
23. Yamaguchi T, Nakayama J. Clinicopathological features of cutaneous lesions of adult T-cell leukemia/lymphoma [Article in Japanese]. *Skin Cancer.* 2006;21(3):268-272.
24. Shimauchi T, Hirokawa Y, Tokura Y. Purpuric adult T-cell leukaemia/lymphoma: expansion of unusual CD4/CD8 double-negative malignant T cells expressing CCR4 but bearing the cytotoxic molecule granzyme B. *Br J Dermatol.* 2005; 152(2):350-352.
25. Adachi A, Kunisada M, Yamada T, et al. Two cases of adult T cell leukemia/lymphoma with petechiae as the first symptom [Article in Japanese]. *Japanese Journal of Clinical Dermatology (Rinsho Hifuka)* 2003;45(3):361-364.
26. Masada M, Nakashima K, Shibazaki Y, et al. Adult T cell leukemia in which petechiae are the only skin manifestation [Article in Japanese]. Clinical Dermatology (Hifuka no Rinsho). 1999;41(8): 1379-1381.
27. Katahira Y, Setoyama M, Tashiro M. Adult T-cell leukemia with purpura [Article in Japanese]. *Practical Dermatology (Hifubyo Shinryo).* 1992;14(3): 255-258.
28. Fukaya T, Yamanaka K, Sato H, et al. A case of various skin manifestations of ATL [Article in Japanese]. *Lymphomas of the Skin (Hifu no Lymphoma).* 1989;8:30-33.
29. Okada J, Imafuku S, Tsujita J, et al. Case of adult T-cell leukemia/lymphoma manifesting marked purpura. *J Dermatol.* 2007;34(11):782-785.
30. Mizutani K, Umezawa Y, Ohta Y, et al. Adult T-cell leukemia with purpura [Article in Japanese]. *Clinical Dermatology (Hifuka no Rinsho).* 2007;49(6): 683-686.
31. Tabata R, Tabata C, Namiuchi S, et al. Adult T-cell lymphoma mimicking Henoch-Schönlein purpura. *Mod Rheumatol.* 2007;17(1):57-62.
32. Nickoloff BJ, Griffiths CE, Baadsgaard O, et al. Markedly diminished epidermal keratinocyte expression of intercellular adhesion molecule-1 (ICAM-1) in Sézary syndrome. *JAMA.* 1989; 261(15):2217-2221.
33. Hashizume H, Nakayama F, Oku T, Takigawa M. Adult T-cell leukemia with regression of erythroderma and simultaneous emergence of leukemia. *J Am Acad Dermatol.* 1992;27(5, pt 2):846-849.
34. Nagatani T, Miyazawa M, Matsuzaki T, et al. Successful treatment of adult T-cell leukemia/lymphoma with MACOP-B, M-FEPA and VEPP-B combination chemotherapy. *J Dermatol.* 1993; 20(10):623-629.

The American Journal of Pathology, Vol. 177, No. 1, July 2010

DOI: 10.2353/ajpath.2010.091120

Epithelial and Mesenchymal Cell Biology

Self-Improvement of Keratinocyte Differentiation Defects During Skin Maturation in ABCA12-Deficient Harlequin Ichthyosis Model Mice

Teruki Yanagi,* Masashi Akiyama,* Hiroshi Nishihara,† Junko Ishikawa,‡ Kaori Sakai,* Yuki Miyamura,* Ayano Naoe,‡ Takashi Kitahara,‡ Shinya Tanaka,§ and Hiroshi Shimizu*

From the Department of Dermatology, Laboratory of Translational Pathology,† the Laboratory of Cancer Research,§ the Department of Pathology, Hokkaido University Graduate School of Medicine, Sapporo; and Tochigi Research Laboratories,‡ Kao Corporation, Ichikai, Haga, Tochigi, Japan*

Harlequin ichthyosis (HI) is caused by loss-of-function mutations in the keratinocyte lipid transporter ABCA12. The patients often die in the first 1 or 2 weeks of life, although HI survivors' phenotypes improve within several weeks after birth. In order to clarify the mechanisms of phenotypic recovery, we studied grafted skin and keratinocytes from *Abca12*-disrupted (*Abca12*$^{-/-}$) mice showing abnormal lipid transport. *Abca12*$^{-/-}$ neonatal epidermis showed significantly reduced total ceramide amounts and aberrant ceramide composition. Immunofluorescence and immunoblotting of *Abca12*$^{-/-}$ neonatal epidermis revealed defective profilaggrin/filaggrin conversion and reduced protein expression of the differentiation-specific molecules, loricrin, kallikrein 5, and transglutaminase 1, although their mRNA expression was up-regulated. In contrast, *Abca12*$^{-/-}$ skin grafts kept in a dry environment exhibited dramatic improvements in all these abnormalities. Increased transepidermal water loss, a parameter representing barrier defect, was remarkably decreased in grafted *Abca12*$^{-/-}$ skin. Ten-passage sub-cultured *Abca12*$^{-/-}$ keratinocytes showed restoration of intact ceramide distribution, differentiation-specific protein expression and profilaggrin/filaggrin conversion, which were defective in primary-cultures. Using cDNA microarray analysis, lipid transporters including four ATP-binding cassette transporters were up-regulated after sub-culture of *Abca12*$^{-/-}$ keratinocytes compared with primary-culture. These results indicate that disrupted keratinocyte differentiation during the fetal development is involved in the pathomechanism of HI and, during maturation, *Abca12*$^{-/-}$ epidermal keratinocytes regain normal differentiation processes. This restoration may account for the skin phenotype improvement observed in HI survivors. *(Am J Pathol 2010, 177:106–118; DOI: 10.2353/ajpath.2010.091120)*

Harlequin ichthyosis (HI) (OMIM 242500) is one of the most severe genetic skin disorders, and its clinical features at birth include severe ectropion, eclabium, flattening of the ears, and large thick plate-like scales over the entire body.[1] Infants affected with HI frequently die within the early neonatal period, although an increasing survival rate for HI newborns has recently been highlighted.[2] In 2005, we and another independent research group identified mutations in the ATP-binding cassette transporter A12 (ABCA12) gene as the cause of HI.[3,4] We previously demonstrated that a severe ABCA12 deficiency causes defective lipid transport in lamellar granules in the upper spinous and granular layer keratinocytes, resulting in malformation of intercellular lipid layers at the granular/cornified layer interface and epidermal lipid barrier disruption resulting in HI phenotype.[3] We recently generated *Abca12*-disrupted (*Abca12*$^{-/-}$) mice by targeting *Abca12*, which closely reproduced the human HI phenotype and died soon after birth.[5] We tried systemic retinoid administration to the pregnant female mice as a form of fetal therapy, although no therapeutic effect was

Supported in part by a grant-in-aid from the Ministry of Education, Science, Sports, and Culture of Japan (Kiban B 20390304: to M.A.), a grant from Ministry of Health, Labor and Welfare of Japan (Health and Labor Sciences Research grants; Research on Intractable Disease: H21–047 and H22-177: to M.A.), a grant from ONO Medical Research Foundation (T.Y.) and a grant from Kanae Foundation for the promotion of Medical Science (T.Y.).

Accepted for publication February 26, 2010.

None of the authors declare any relevant financial relationships.

Supplemental material for this article can be found on *http://ajp.amjpathol.org*.

Address reprint requests to Masashi Akiyama, M.D., Ph.D., or Hiroshi Shimizu, M.D., Ph.D., Department of Dermatology, Hokkaido University Graduate School of Medicine, N15 W7, Kita-ku, Sapporo 060-8638, Japan. E-mail: akiyama@med.hokudai.ac.jp or shimizu@med.hokudai.ac.jp.

obtained in the *Abca12*$^{-/-}$ newborns after treatment.[5] After our publication, Zuo et al[6] also reported another *Abca12* knockout mouse, whose skin showed similar features to our model mice.

Previously, we demonstrated severe skin barrier defects in *Abca12*$^{-/-}$ mice and suggested that "barrier insufficiency" plays an important role in HI phenotype expression.[5] However, "the barrier insufficiency" theory fails to completely explain the pathomechanism of the HI phenotype. HI fetuses show a HI phenotype even *in utero*, where skin barrier protection against a dry environment is not required. In addition, the skin phenotype of HI long-term survivors maintained in a dry environment shows a dramatic improvement within several weeks after birth where they require a normal skin barrier function. Thus, we suspected that other unknown mechanisms are involved in HI and the formation HI survivors' skin phenotypes. To date there have been no reports which have compared the skin phenotypes in fatally affected HI neonates and survivors, and the exact mechanism of HI survivors' skin phenotype improvement has yet to be clarified. Thus, we have carefully analyzed the keratinization process of neonatal versus grafted HI model mice skin and primary versus subcultured *Abca12*$^{-/-}$ keratinocytes instead of human HI neonatal and survivors' skin. Initially, we investigated the distribution and amounts/composition of lipids, and expression of differentiation-specific molecules in neonatal HI model mice skin. Then, we studied the alteration of them in grafted HI model mouse skin transplanted onto severe combined immunodeficient (SCID) mice. In addition, we performed keratinocyte culture experiments including immunostaining and Western blotting using primary/subcultured *Abca12*$^{-/-}$ keratinocytes to confirm the results of the neonatal and grafted skin experiments. Further, we analyzed the whole gene expression profile of primary versus subcultured *Abca12*$^{-/-}$ keratinocytes using cDNA microarray methods. Finally, we conducted therapeutic trials on primary-cultured *Abca12*$^{-/-}$ keratinocytes and grafted HI model mice skin with retinoids.

Materials and Methods

Animals

All animal studies were reviewed and approved by the Animal Use and Care Committee of the Hokkaido University Graduate School of Medicine. C57BL/6 strain mice and SCID mice were purchased from Clea (Tokyo, Japan). All animals used for this study were maintained under pathogen-free conditions.

Antibodies

Rabbit polyclonal affinity purified anti-mouse Abca12 antibody was raised in rabbits using a 14-amino acid sequence synthetic peptide (residues 2581 to 2594) derived from the mouse Abca12 sequence (XM001002308) as the immunogen.[5] The other primary antibodies were rabbit anti-profilaggrin/filaggrin antibody (COVANCE, Princeton, NJ), rabbit anti-involucrin antibody (M-116; Santa Cruz Biotechnology, Santa Cruz, CA), rabbit anti-desmoglein 1 antibody (H-290; Santa Cruz Biotechnology), rabbit anti-mouse loricrin antibody (AF62; COVANCE), rabbit anti-kallikrein 5 antibody (ab7283; Abcam, Cambridge, UK), rabbit anti-glucosylceramide/ceramide antibody (Glycobiotech, Kukels, Germany), and mouse monoclonal anti-β actin antibody (Sigma Chemical Co., St. Louis, MO). Secondary antibodies used in the present study were as follows; Alexa Fluor 488-conjugated donkey anti-rabbit IgG (Invitrogen Corp., Carlsbad, CA), fluorescein isothiocyanate-conjugated goat anti-rabbit IgG (Jackson Immuno Research, West Grove, PA), horseradish peroxidase-conjugated goat anti-rabbit IgG or horseradish peroxidase-conjugated goat anti-mouse IgG (Invitrogen Corp.).

Generation of Abca12$^{-/-}$ *Mouse*

The procedure for generating *Abca12*$^{-/-}$ mice has been previously described.[5] Briefly, we cloned mouse genomic DNA Abca12 fragments from the mouse 129Sv/Ev genomic library (Bacpac Resources Center, Children's Hospital Oakland Research Institute, Oakland, CA). We subcloned a 10.6-kb fragment to make the targeting vector. We inserted the PGK/Neo cassette between 47 bp upstream of the exon 30 and 203 bp downstream of exon 30. We transfected the targeting vector by electroporation into 129Sv/Ev embryonic stem cells, then microinjected the correctly targeted embryonic stem cell line into blastocysts obtained from C57BL/6 mice to generate chimeric mice, which we then mated with C57BL/6 females. We crossed the heterozygotes with C57BL/6 over at least five generations, and then intercrossed them to generate the *Abca12*$^{-/-}$ mice. Genotyping was performed by PCR as described previously.[5]

Establishment of Abca12$^{-/-}$ *Mice Keratinocyte Culture*

Skin samples from *Abca12*$^{-/-}$ and wild-type mice were processed for primary keratinocyte culture, and cells were grown according to standard procedures in CnT-57 medium (Cellntec Advanced Cell Systems, Bern, Switzerland). For differentiation induction, culture medium was switched from CnT-57 medium to CnT-02 medium (Cellntec Advanced Cell Systems) and, 24 hours later, the calcium concentration was changed to 1.2 mmol/L. 48 hours later, we performed extractions of total RNA and protein from cultured cells. We established primary-cultured keratinocytes from two *Abca12*$^{-/-}$ mice and two wild-type mice.

Skin Grafting

In total, ten *Abca12*$^{-/-}$ and three wild-type neonates were sacrificed by anesthesia with ether inhalation, and their dorsal skin excised and transplanted onto SCID mice (Clea). Those skin grafts were fully adapted within 2 weeks after grafting. At 3 weeks after transplantation, the skin grafts were harvested for further analysis.

Extraction of Total RNA and Real-Time Reverse Transcriptase PCR Analysis

We separated the epidermis from whole skin samples of wild and *Abca12−/−* mice by 1 mol/L NaCl in sterile water at 4°C for 2 hours. We isolated total RNA from the epidermis using the Quick Gene RNA Tissue Kit SII (Fujifilm Corp, Tokyo, Japan). We also isolated total RNA from keratinocytes cultured from wild-type and *Abca12−/−* skin using the RNeasy mini kit (Qiagen Corp, Tokyo, Japan). RNA concentration was measured spectrophotometrically and samples were stored at −80°C until use for reverse transcriptase PCR. We reverse-transcribed RNA using Superscript II (Invitrogen Corp.) following the manufacturer's instructions. Complementary DNA samples were analyzed by ABI prism 7000 sequence detection system (Applied Biosystems, Foster City, CA). Primers and probes specific for differentiation-specific protein genes including loricrin, kallikrein 5, transglutaminase 1, involucrin, filaggrin, and control house keeping genes, glyceraldehyde-3-phosphate dehydrogenase (GAPDH), and β-actin, were obtained from Taqman Gene Expression Assay (Applied Biosystems) (Probe ID; Mm01962650_s1, Mm01203811_a1, Mm00498375_a1, Mm00515219_s1, Mm01716522_m1, Mm99999915_g1, and Mm00607939_s1). Differences between the mean CT values of loricrin, kallikrein 5, transglutaminase 1, involucrin, filaggrin and those of GAPDH or β-actin were calculated as: ΔCT*Abca12−/−* mice = CTloricrin (or other keratinization markers) − CTGAPDH (or other house keeping genes) and those of ΔCT for the *Abca12+/+* asΔCT calibrator = CTloricrin (or other keratinization markers) − CTGAPDH (or other house keeping genes).

We could obtain the similar results from GAPDH and β-actin standard, thus we described the results of GAPDH standard in the present study. Final results for *Abca12*$^{-/-}$ mouse samples/wild-type mouse samples (%) were determined by $2^{-(}$ΔCTAbca12−/− sample − ΔCTcalibrator). We measured mRNA levels five times for each clones. Using similar methods, we quantitatively analyzed these differentiation-specific mRNA expression levels in the primary/subcultured keratinocytes from *Abca12*$^{-/-}$ and wild-type mice.

Western Blotting

We separated the epidermis from whole skin samples of wild and *Abca12*$^{-/-}$ mice by 1mol/L NaCl in sterile water at 4°C for 2 hours. For Western blotting, we used epidermal homogenates and proteins extracted from cultured keratinocytes prepared with radioimmunoprecipitation assay (RIPA) buffer comprising 50 mmol/L Tris-HCl, pH7.5, 150 mmol/L NaCl, 1% Nonidet P-40, 0.5% deoxycholate, 0.1% SDS, and Roche protease cocktail tablet (Roche, Basel, Switzerland). Protein concentrations were measured using Micro BCA protein assay kit (Thermo Scientific, Rockford, IL). Protein concentration of the samples for western blotting was from 1 to 2 μg/μl. The 20 μg protein loading per single lane was separated by a 5 to 20% gradient gel SDS-polyacrylamide gel and transferred to polyvinylidene difluoride membranes. Membrane blocking and incubation with antibodies were performed in Tris-buffered saline with 2% nonfat dry milk. Signals were revealed with chemiluminescence reagents and photographed by LAS-1000 mini (Fujifilm Corp, Tokyo, Japan). We also confirmed the loading protein dose by β-actin antibody staining as internal protein control. For analysis of filaggrin solubility and processing, epidermal lysates were prepared with RIPA buffer. Samples of precipitated proteins in the RIPA buffer were solubilized again in 8 mol/L urea before boiling in reducing SDS loading buffer.

Light Microscopy and Immunofluorescence Analysis

For light microscopy, we harvested the newborn pups' skin and the grafted skin, and fixed them for 24 hours in 10% neutral buffered formalin, dehydrated them in graded ethanol, and embedded them in paraffin. We cut 4-μm sections and stained them with H&E. For immunohistochemistry, the tissue samples were embedded in optimal cutting temperature compound (Sakura Finetechnical Corp., Tokyo, Japan). Frozen tissue sections were cut at a thickness of 5 μm. The sections were blocked with 1% bovine serum albumin (BSA) in PBS for 30 minutes at room temperature, and incubated in primary antibody solution in blocking buffer for 30 minutes at 37°C. Fluorescent labeling was performed with secondary antibodies, followed by propidium iodide (Sigma Chemical Co.) for 5 minutes at room temperature to counterstain nuclei. The stained samples were observed under an Olympus Fluoview confocal laser-scanning microscope (Olympus, Tokyo, Japan).

In Situ *Transglutaminase Activity*

The procedure for *in situ* transglutaminase 1 activity assay has been previously described.[7,8] In brief, unfixed cryosections of 5 μm were blocked with 100 mmol/L Tris-HCl pH7.4, 1% BSA for 30 minutes, and then incubated with 100 mmol/L Tri-HCl pH7.4, 5 mmol/L $CaCl_2$, 12 μmol/L monodansylcadaverine (Sigma) for 1 hour to detect transglutaminase 1 activity. For negative controls, EDTA was added to the monodansylcadaverine solution to a final concentration of 20 mmol/L. After stopping the transglutaminase 1 reaction with 10 mmol/L EDTA in PBS, sections were incubated with rabbit anti-dansyl antibody (Invitrogen Corp.) in 12% BSA/PBS for 3 hours. Sections were then incubated with fluorescein isothiocyanate-conjugated goat anti-rabbit antibody in 12% BSA/PBS for 30 minutes. Nuclei were counterstained by propidium iodide. The stained samples were observed under an Olympus Fluoview confocal laser-scanning microscope (Olympus).

Immunofluorescence Labeling of Cultured Cells

Immunofluorescence labeling of cultured cells was performed as previously described.[5] Briefly, primary/subcultured keratinocytes were fixed in 4% paraformaldehyde for 15 minutes and permeabilized with 0.1% Triton X-100 for 15 minutes at room temperature. Keratinocytes were blocked with 1% BSA in PBS for 30 minutes at room temperature,

and incubated in primary antibody solution in blocking buffer for 30 minutes at 37°C and fluorescence labeling was performed with secondary antibodies, followed by propidium iodide for 5 minutes at room temperature to counterstain nuclei. The stained samples were observed under an Olympus Fluoview confocal laser-scanning microscope (Olympus).

Electron Microscopy

Neonatal skin samples and skin grafts were fixed in 5% glutaraldehyde solution, post fixed in 1% OsO_4, dehydrated, and embedded in Epon 812 (TAAB Laboratories, Berkshire, UK). All of the samples were ultra-thin sectioned at a thickness of 70 nm, and stained with uranyl acetate and lead citrate. Photographs were taken using a Hitachi H-7100 transmission electron microscope (Hitachi, Tokyo, Japan).

Lipid Analysis

Lipid analysis was performed as previously reported.[9] Briefly, lipid analysis was done independently on three *Abca12*$^{-/-}$ neonates, two wild-type as controls, and two mature *Abca12*$^{-/-}$ skins 3 months after skin grafting and two mature wild-type skins 3 months after transplantation as control. We separated the epidermis from whole skin specimens of control and *Abca12*$^{-/-}$ mice by incubation in sterile water at 60°C for 1 minute and homogenized in 0.8 ml of PBS. A total lipid component was extracted from tissue homogenates of epidermis according to conventional methods.[9] Lipid analysis in epidermal lysates from neonates and grafted skin was performed by liquid chromatography, electrospray ionization mass spectrometry (LC-ESI-MS) using a HP 1100 liquid chromatography system (Agilent Technologies, Palo Alto, CA).

Measurement of Transepidermal Water Loss

Transepidermal water loss (TEWL) from the skin of neonatal mice and from skin grafted onto SCID mice was measured by evaporimeter (AS-VT100RS: Asahibiomed Corp., Yokohama, Japan), as described previously.[5] The AS-VT100RS utilizes the ventilated-chamber method for measuring TEWL. Its hygrometer measures the humidity of incoming air and of outgoing air that has passed over the test area of the skin, and TEWL is calculated from the difference. TEWL measurements were performed on the back of the neonates and the grafted skin onto the back of SCID mice.

Complementary DNA Microarray Analysis for the Gene Expression Profile

Total RNA isolated from primary/subcultured *Abca12*$^{-/-}$ keratinocytes was extracted as described above. Total RNA concentration was calculated spectrophotometrically, and quality control of RNA was analyzed with an Agilent 2100 Bioanalyzer (Agilent Technologies, Tokyo, Japan). mRNA/cDNA hybrids were generated via T7oligo dT primers, followed by addition of DNA polymerase and ligase (Filgen, Nagoya, Japan) to obtain double-stranded cDNA. The sample tagged with chemiluminescent substrate, Cy3 for the subcultured *Abca12*$^{-/-}$ keratinocytes, or Cy5 for the primary-cultured *Abca12*$^{-/-}$ keratinocytes, was hybridized on a microarray chip (Filgen Array mouse 32K, Filgen). We used a mixture of total RNAs from the two cultures for labeling reactions. Fluorescence images for Cy3 and Cy5 dye channels were obtained using a GenePix 4000B scanner (Axon Instruments, CA) and scan data images were analyzed using Microarray Data Analysis Tool version 3.0 software (Filgen).

Therapeutic Trial with Retinoids on Primary-Cultured Abca12$^{-/-}$ *Keratinocytes and Grafted Harlequin Ichthyosis Model Mice Skin*

To test the efficacy of a therapeutic trial on primary-cultured *Abca12*$^{-/-}$ keratinocytes, isotretinoin (purchased by Sigma Chemical Co., St. Louis, MO) was dissolved in dimethyl sulfoxide (DMSO). In addition, etretinate powder (a gift from Chugai Pharmaceuticals, Tokyo, Japan) was dissolved in sterile water.

Primary-cultured keratinocytes were grown in CnT-57 medium (Cellntec Advanced Cell Systems) and then switched into CnT-02 medium (Cellntec Advanced Cell Systems). Twenty-four hours later, the calcium concentration was changed to 1.2 mmol/L in CnT-02 medium with retinoids (10^{-6}mol/L isotretinoin or 10^{-6}mol/L etretinate) dissolved in DMSO or water. The final concentration of DMSO in medium was 0.01%. As control, keratinocytes were cultured in CnT-02 medium with 1.2 mmol/L calcium supplemented with 0.01% DMSO without retinoids. Forty-eight hours later, we extracted protein from keratinocytes.

In a therapeutic trial using grafted HI model mice skin, we dissolved several doses of isotretinoin in soy oil, and single doses (1, 10 mg/kg) of isotretinoin were administered orally into the grafted SCID mice 3 weeks after skin transplantation every day for 10 days.

Statistical Analysis

All statistical analyses were performed using student's *t*-tests with sample sizes indicated in the figure legends for each comparison that was made. *P* values of <0.05 were considered statistically significant.

Results

Abca12$^{-/-}$ *Neonatal Mouse Epidermis Exhibited Defective Lipid Distribution, Reduced Expression of Differentiation-Specific Proteins and Profilaggrin/Filaggrin Conversion Defects*

As we previously reported,[5] *Abca12*$^{-/-}$ mice (Figure 1B) were typically born with a smaller body size than that of wild-type mice (Figure 1A). Erythematous, rigid skin covered the entire body surface of *Abca12*$^{-/-}$ neonates.

Light microscopy showed a thick, compact cornified layers without the normal basket-weave appearance in the *Abca12*$^{-/-}$ neonatal skin (Figure 1D), compared with normal neonatal skin (Figure 1C). Electron microscopy of *Abca12*$^{-/-}$ neonatal skin showed numerous lipid droplets in the granular layer cell cytoplasm (Figure 1F). In wild-type neonatal skin, no lipid droplets were seen although normal keratohyalin granules were observed (Figure 1E). Immunofluorescence staining (Figure 1, G and H) showed Abca12 in wild-type but not abca12−/− mice, with the glucosylceramide/ceramide distribution remarkably sparse at the *Abca12*$^{-/-}$ neonatal mice granular/cornified layer interface (Figure 1J), compared with the intense labeling in the wild-type neonatal epidermis (Figure 1I). To verify these results in the neonatal *Abca12*$^{-/-}$ and wild-type skin, we performed lipid analysis using skin samples from both the *Abca12*$^{-/-}$ and wild-type neonates. Total amounts of epidermal ceramides were significantly reduced in *Abca12*$^{-/-}$ neonatal mice (Figure 1K). Particularly, amounts/compositions of the CER[EOS], ceramide classes consisting of ester-linked non-hydroxy fatty acids, ω-hydroxy fatty acids and 4-sphinnenines, in *Abca12*$^{-/-}$ neonatal epidermis were extremely small compared with control mice (see Supplemental Figure S1, A and B at *http://ajp.amjpathol.org*).

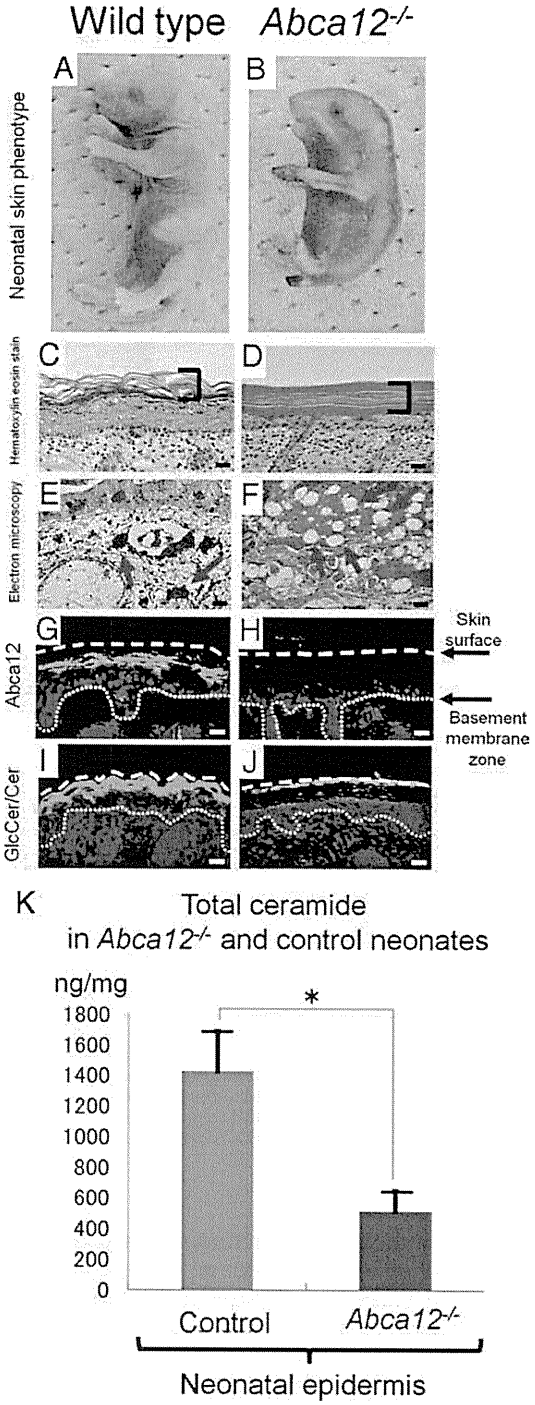

Immunofluorescence staining revealed that the keratinocyte differentiation (keratinization)-specific molecules, kallikrein 5 (KLK5), transglutaminase 1 (TGase1), and loricrin, were sparsely distributed in the upper epidermis of neonatal *Abca12*$^{-/-}$ mice (Figure 2A–J). Immunofluorescence staining for KLK5, a lamellar granule component, was weak in *Abca12*$^{-/-}$ neonatal mice granular layer (Figure 2B), in contrast to intense labeling in granular and lower cornified layers of wild-type neonatal skin (Figure 2A). *In situ* TGase1 activity assays with dansylcadaverine as a substrate showed neonatal *Abca12*$^{-/-}$ granular layer keratinocytes exhibited weak TGase1 activity restricted to the cytoplasm (Figure 2D), compared with distinct TGase1 activity with a more peripheral pattern throughout neonatal wild-type granular layer keratinocytes (Figure 2C). Immunofluorescence staining showed loricrin expressed sparsely within neonatal *Abca12*$^{-/-}$ granular layer cells (Figure 2F), compared with more intense expression in neonatal wild-type granular layer keratinocytes (Figure 2E).

KLK5, involucrin, TGase1, loricrin, and filaggrin mRNA expression was up-regulated in neonatal *Abca12*$^{-/-}$ epidermal keratinocytes (Figure 2K). In contrast, protein expression using epidermal extract, Western blotting demonstrated that loricrin and KLK5 protein expression was reduced in neonatal *Abca12*$^{-/-}$ epidermal keratinocytes compared with that in neonatal wild-type epidermis (Figure 2L). There were no significant differences in the pro-

Figure 1. *Abca12*$^{-/-}$ neonatal phenotype and lipid trafficking defects. **A** and **B:** Gross phenotypes of wild-type and *Abca12*−/− neonates. **C** and **D:** Light microscopy showed a thick compact cornified layer (bracket) without the normal basket-weave appearance in the *Abca12*$^{-/-}$ mouse skin (**D**), compared with normal neonatal skin (**C**) (H&E stain; original magnification, ×40) (Scale bars = 20 μm). **E** and **F:** An electron micrograph of the *Abca12*−/− neonatal skin showed numerous lipid droplets in the cytoplasm of the granular layer cells (**F, red arrows**). In the wild-type neonatal skin, no lipid droplets were seen and normal keratohyalin granules were observed (**E, red arrows**) (original magnification, ×3000) (Scale bars = 2 μm). **G** and **H:** By immunofluorescence staining, Abca12 expression (Alexa488, green) was detected in the wild-type neonatal mouse skin (**G**), but not in the *Abca12*$^{-/-}$ skin (**H**). **I** and **J:** Immunofluorescence staining showed the glucosylceramide/ceramide (GlcCer/Cer) (Alexa 488, green), a major lipid component of lamellar granules and an essential component of the epidermal permeability barrier, to be distributed remarkably sparse in the *Abca12*−/− neonatal mouse granular/cornified layer interface (**J**), compared with the intense labeling in the wild-type neonatal epidermis (**I**). **K:** In neonatal mice, total ceramides levels were significantly reduced in the epidermis of *Abca12*$^{-/-}$ mice. (*Abca12*−/− neonates, $n = 3$; control neonates, $n = 2$) (*$P < 0.01$). GlcCer, glucosylceramide; Cer, ceramide.

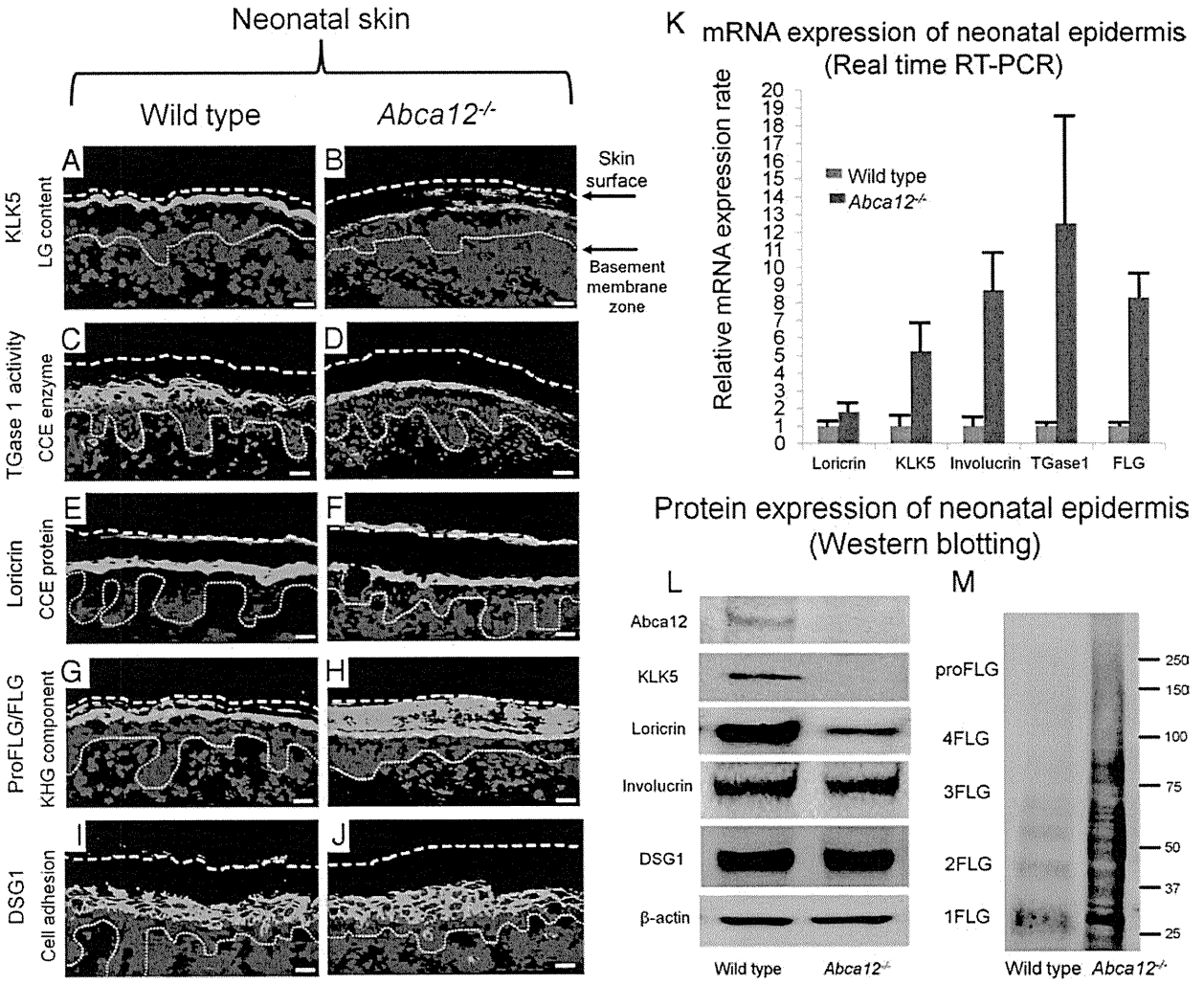

Figure 2. Reduced epidermal differentiation-associated molecules and defective conversion of profilaggrin to filaggrin in *Abca12*$^{-/-}$ neonates. **A** and **B:** Immunofluorescence staining for kallikrein 5 (KLK5) (Alexa488, green), one of the lamellar granule (LG) contents, was weak in the *Abca12−/−* neonatal mice granular keratinocyte layers (**B**), in contrast to its intense labeling in the granular layers and lower cornified layers of wild-type neonatal skin (**A**). **C** and **D:** *In situ* transglutaminase 1 (TGase1) activity assay (fluorescein isothiocyanate, green) with dansyl-cadaverine showed the granular layer keratinocytes in the *Abca12*$^{-/-}$ neonates had weak transglutaminase 1 activity only in the cytoplasm (**D**), compared with distinct transglutaminase 1 activity with the peripheral pattern throughout granular layer keratinocytes in the wild-type neonates (**C**). Cytoplasmic localization of transglutaminase 1 in *Abca12−/−* neonates indicated its inability to bind to the cell membrane and to therefore function at its proper place despite the significantly enhanced mRNA expression of transglutaminase 1 (see Figure 2K). **E** and **F:** Immunofluorescence staining showed loricrin (Alexa 488, green) expressed sparsely in the *Abca12*$^{-/-}$ neonatal mice granular layer (**F**), compared with its intense expression in the granular layer of the wild-type neonatal skin (**E**). **G** and **H:** Both *Abca12−/−* and wild-type neonatal skin showed intense profilaggrin/filaggrin (proFLG/FLG) (Alexa488, green) expression in the granular layer keratinocytes. However, in *Abca12*$^{-/-}$ neonatal skin, profilaggrin/filaggrin distribution was also observed throughout the cornified layers. **I** and **J:** Desmoglein 1(DSG1) (Alexa 488, green), a cell adhesion molecule unassociated with keratinization, was expressed at the cell periphery in the lower granular and spinous layers of the both *Abca12−/−* neonatal skin and wild-type mouse skin. (nuclear stain; propidium iodide, red, **dotted lines**, the skin surface). Original magnification ×40; Scale bars, 20 μm. **K:** mRNA expression of loricrin, kallikrein 5 (KLK5), involucrin, transglutaminase 1 (TGase1) and filaggrin (FLG) was up-regulated in the *Abca12*$^{-/-}$ neonatal epidermis. (*Abca12−/−* neonates, $n = 5$; wild-type neonates, $n = 5$, mRNA expression levels of wild-type neonatal epidermis = 1). **L:** Western blotting of epidermal extracts showed that protein expression of kallikrein 5 (KLK5) and loricrin was lower in the *Abca12*$^{-/-}$ neonatal epidermis (right) than in the wild-type neonatal epidermis (left). There were no significant differences of desmoglein 1(DSG1), involucrin, β-actin expressions between the *Abca12−/−* and wild-type epidermis. **M:** Western blotting with anti-profilaggrin/filaggrin antibody revealed the *Abca12*$^{-/-}$ neonatal epidermis (right) expressed more profilaggrin/filaggrin protein than wild-type neonatal epidermis (left). High molecular weight smear band corresponding to non-converted profilaggrin peptides were characteristic to the *Abca12−/−* neonatal epidermis. Western blotting using serial protein dilutions is shown in the supplemental Figure 2 (see Supplemental Figure S2 at *http://ajp.amjpathol.org*). KLK5, kallikrein 5; LG, lamellar granule; TGase1, transglutaminase 1; CCE, cornified cell envelope; FLG, filaggrin; KHG, keratohyalin granule; DSG1, desmoglein 1; proFLG, profilaggrin; 4FLG, filaggrin tetramer; 3FLG, filaggrin trimer; 2FLG, filaggrin dimer; 1FLG, filaggrin monomer.

tein expression of involucrin or control molecules unconnected with the keratinization process, β-actin, and desmoglein1 (DSG1), between *Abca12*$^{-/-}$ and wild-type neonatal epidermis.

Both *Abca12*$^{-/-}$ and wild-type neonatal skin demonstrated intense profilaggrin/filaggrin expression within granular layer keratinocytes (Figure 2, G and H). However, in *Abca12*$^{-/-}$ neonatal skin, profilaggrin/filaggrin distribution was also observed throughout all of the cornified layers (Figure 2H). Western blotting with anti-profilaggrin/filaggrin antibody revealed that neonatal *Abca12*$^{-/-}$ epidermis exhibited a greater amount of profilaggrin/filaggrin protein than that in the neonatal wild-type epidermis (Figure 2M). In particular, high molecular weight smear bands correspond-

ing to unconverted profilaggrin peptides were characteristic of neonatal *Abca12*$^{-/-}$ epidermis. Western blotting using the serial dilutions of protein showed that neonatal *Abca12*$^{-/-}$ epidermis exhibited a filaggrin monomer band, although the ratio of high molecular weight profilaggrin and its derivatives to filaggrin monomer in the *Abca12*$^{-/-}$ neonatal epidermis was extremely high compared with that of the wild-type neonatal epidermis (see Supplemental Figure S2A at *http://ajp.amjpathol.org*). The remaining high molecular bands in the neonatal *Abca12*$^{-/-}$ epidermis indicated defective profilaggrin conversion to filaggrin. Furthermore, we prepared 8 mol/L urea supernatants from precipitated proteins from the *Abca12*$^{-/-}$ neonatal epidermis in RIPA buffer. Western blotting with 8 mol/L urea supernatants confirmed that a proportion of filaggrin monomer, which is insoluble in the RIPA buffer exists in *Abca12*$^{-/-}$ neonatal epidermis (see Supplemental Figure S2B at *http://ajp.amjpathol.org*). In contrast, urea supernatants from precipitated proteins in RIPA buffer of wild-type neonatal epidermis showed only a faint band of filaggrin monomer. This finding indicated that majority of filaggrin monomer in the wild-type neonatal epidermis is soluble in RIPA buffer. These Western blotting results suggested that *Abca12*$^{-/-}$ neonatal epidermis exhibited not only defective profilaggrin/filaggrin conversion but also alteration of filaggrin monomer solubility. We also performed Western blotting with anti-loricrin antibody using 8 mol/L urea supernatant. Using 8 mol/L urea buffer as well as using RIPA buffer the loricrin band was faint in supernatant samples from the *Abca12*$^{-/-}$ neonatal epidermis (data not shown). Thus, the solubility of loricrin was unaltered in the *Abca12*$^{-/-}$ neonatal epidermis and we think that the alteration of solubility in the *Abca12*$^{-/-}$ neonatal epidermis is specific to filaggrin.

Improved Morphological Abnormalities, Corrected Lipid Distribution, and Restored Expression of Differentiation-Specific Molecules in Abca12$^{-/-}$ *Skin Grafts Maintained in Dry Environment*

Since *Abca12*$^{-/-}$ neonates die soon after birth, it was impossible to follow the phenotypic changes in the skin of *Abca12*$^{-/-}$ mice after birth. Therefore, we grafted their skin onto severe combined immunodeficient (SCID) mice and analyzed its morphological and biochemical alterations in the skin after birth/grafting.

Mature grafted *Abca12*$^{-/-}$ skin showed hairless keratotic plates at 3 weeks after transplantation onto the backs of SCID mice (Figure 3, A and B). Light microscopic observations revealed that hair follicles and shafts were buried in keratotic plugs in mature *Abca12*$^{-/-}$ skin (Figure 3, C and D). High power microscopy demonstrated that mature *Abca12−/−*skin showed discernible keratohyalin granules in the granular layers (Figure 3F) that were completely absent in *Abca12*$^{-/-}$ neonatal skin (Figure 1, E and F).

Immunofluorescence staining showed abca12 staining in wild-type but not abca12−/−mice and intense labeling of glucosylceramides/ceramides at the granular/cornified layer interface in mature grafted *Abca12*$^{-/-}$ skin (Figure 3, I and J), compared with a sparse distribution in the neonatal *Abca12−/−* mouse upper epidermis (Figure 1L). Electron microscopy of mature *Abca12*$^{-/-}$ skin showed many lipid droplets in the granular layer (Figure 3K), although the number of lipid droplets in the cornified layer was reduced when compared with that of neonatal skin (Figure 3L). Using lipid analysis, the amounts of both total ceramides and CER[EOS] were restored in mature *Abca12−/−* epidermis (Figure 3M, and see Supplemental Figure S1, C and D at *http://ajp.amjpathol.org*). These results indicate that mature grafted *Abca12*$^{-/-}$ epidermis was able to obtain a normal ceramide distribution together with a normal composition of ceramides.

Immunolabeling for differentiation-specific molecules confirmed improved keratinization during maturation of the grafted *Abca12*$^{-/-}$ skin (Figure 4, A–J). Intense KLK5 immunolabeling (Figure 4, A and B), *in situ* transglutaminase 1 (TGase1) activity (Figure 4, C and D), and loricrin immunostaining (Figure 4, E and F) were distributed throughout the granular layers in mature grafted *Abca12−/−* skin, compared with a sparse distribution in *Abca12*$^{-/-}$ neonatal skin (Figure 2, B, D, and F). Increased loricrin and KLK5 immunolabeling intensity was confirmed by Western blot analysis using epidermal extracts from mature grafted *Abca12−/−* epidermis (Figure 4K).

Mature grafted *Abca12*$^{-/-}$ skin showed intense profilaggrin/filaggrin labeling in the granular layer (Figure 4H), similar to the mature grafted wild-type skin (Figure 4G). The diffuse profilaggrin/filaggrin distribution throughout the cornified layers observed in *Abca12−/−* neonatal skin (Figure 2H) was not seen in mature grafted *Abca12*$^{-/-}$ skin (Figure 4H). Western blotting with anti-profilaggrin/filaggrin antibody revealed that the normal conversion of profilaggrin to filaggrin was restored in mature *Abca12−/−* epidermis (Figure 4K). Epidermal extracts of mature *Abca12*$^{-/-}$ skin at 3 weeks after transplantation showed low expression of high molecular weight smeared bands and, instead of those, exhibited intense filaggrin monomer bands, compared those with epidermal extracts of *Abca12−/−* neonatal skin.

Analysis of TEWL as a parameter of skin barrier defects, demonstrated *Abca12*$^{-/-}$ that neonatal back skin showed significantly greater TEWL than the wild-type neonatal skin ($n = 3$, $P < 0.001$) (Figure 4L). However, TEWL levels of mature *Abca12−/−* skin 3 weeks after the skin graft were significantly decreased as compared with levels of *Abca12*$^{-/-}$ neonatal skin ($n = 3$, $P < 0.001$).

Subcultured Abca12$^{-/-}$ *Mouse Keratinocytes Attained Normal Lipid Trafficking in the Cytoplasm, with Restoration of Differentiation-Specific Protein Expression and Intact Profilaggrin/ Filaggrin Conversion that Was Defective in Primary-Cultured* Abca12−/− *Mouse Keratinocytes*

To verify the results from grafted skin analysis, we performed a similar analysis using primary versus subcultured *Abca12*$^{-/-}$ keratinocytes. Immunolabeling with an-

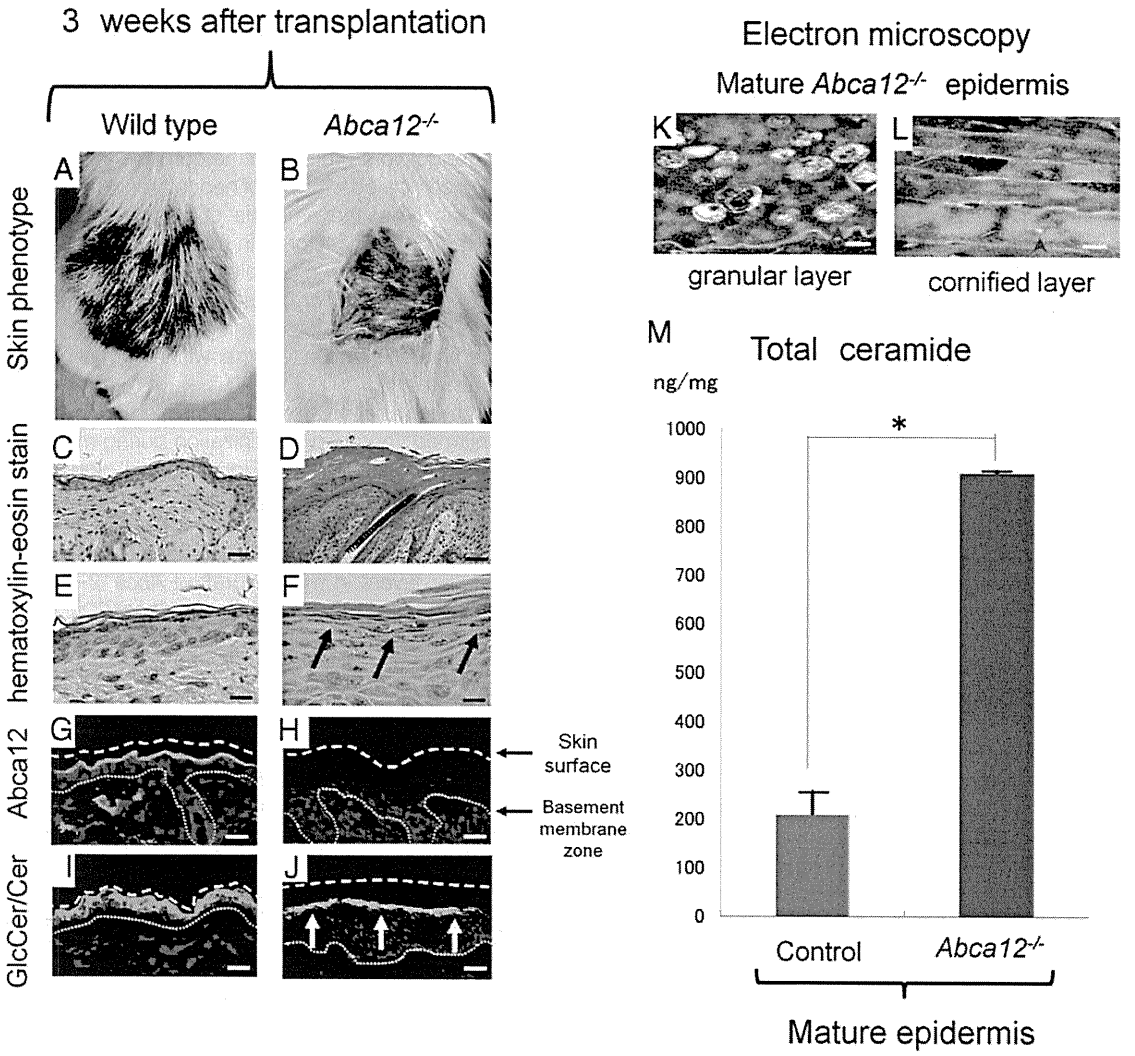

Figure 3. Altered morphology and improvement of ceramide deficiency during maturation of *Abca12*$^{-/-}$ skin. Gross (**A** and **B**) and microscopic (**C–L**) appearances of wild-type and *Abca12−/−* skin three weeks after transplantation onto SCID mice. **A:** Grafted skin of wild-type mice three weeks after transplantation. **B:** Grafted *Abca12*$^{-/-}$ skin three weeks after transplantation showed hairless keratotic plates. **C** and **D:** Light microscopic observation histology (H&E stain; original magnification ×40; Scale bars = 20 μm). Hair follicles and shafts were buried in keratotic plugs in the mature *Abca12−/−* skin three weeks after the skin graft (**D**). **E** and **F:** High power views (H&E stain; original magnification ×60; Scale bars = 10 μm). Mature *Abca12*$^{-/-}$ skin three weeks after transplantation showed discernible keratohyalin granule in the granular layers (**F, arrows**) that were lacked in *Aba12−/−* neonatal skin (see Figure 1, D and F). **G** and **H:** By immunofluorescence staining, Abca12 expression (Alexa488, green) was detected in the mature wild-type mouse skin (**G**), but not in the mature *Abca12*$^{-/-}$ skin (**H**). **I** and **J:** Immunofluorescence staining showed an intense distribution of glucosylceramide/ceramide (GlcCer/Cer) (Alexa 488, green) at the granular/cornified layer interface in mature *Abca12−/−* epidermis (**J, arrows**), compared with a sparse distribution in the neonatal *Abca12*$^{-/-}$ mouse upper epidermis (see Figure 1J). **K** and **L:** Ultrastructural observation of the grafted *Abca12−/−* skins three weeks after transplantation. There were many lipid droplets in the granular layer (**K, red arrowheads**), however the number of lipid droplets in the cornified layer (**L, red arrowheads**) was fewer than that of the neonatal *Abca12*$^{-/-}$ skin (see Figure 1F). Original magnification: ×10000 (**K**), ×5000 (**L**); Scale bars: 100 nm (**K**), 200 nm (**L**). **M:** From the lipid analysis of grafted skins, total ceramides levels of mature *Abca12*$^{-/-}$ epidermis were restored. (*Abca12−/−* grafted skins, $n = 2$; control grafted skins, $n = 2$) (*$P < 0.01$). GlcCer, glucosylceramide; Cer, ceramide

ti-glucosylceramide/ceramide antibody demonstrated a congested glucosylceramide/ceramide pattern in differentiated primary-cultured *Abca12−/−* mouse keratinocytes after first passage (Figure 5, B and E), compared with an uncongested, diffuse peripheral glucosylceramide/ceramide pattern in differentiated primary-cultured wild-type mouse keratinocytes (Figure 5, A and D). After 10 passages, subcultured *Abca12*$^{-/-}$ keratinocytes showed a widely distributed, diffuse glucosylceramide/ceramide staining pattern, similar to those of primary-cultured wild-type keratinocytes (Figure 5, C and F). Subcultured wild-type keratinocytes after 10 passages failed to show any alterations in lipid distribution (data not shown). These results indicate that lipid trafficking recovered during 10 passages of subculture in our *Abca12−/−* keratinocytes.

To investigate this altered differentiation state of primary/subcultured *Abca12*$^{-/-}$ keratinocytes, we performed real-time RT-PCR and immunoblot analysis (Figure 5, G and H). No significant differences were obtained in loricrin, KLK5, involucrin, TGase1 and filaggrin mRNA expression between primary-cultured *Abca12−/−* and wild-type keratinocytes (Figure 5G). Subcultured *Abca12*$^{-/-}$ keratinocytes showed higher loricrin, KLK5 and TGase1 mRNA